Mathematical Biosciences and Engineering

https://www.aimspress.com/journal/mbe

MBE, 22(10): 2641–2671.
DOI: 10.3934/mbe.2025097
Received: 24 May 2025
Revised: 05 August 2025
Accepted: 05 August 2025
Published: 25 August 2025

Research article

Integrating stochastic chemotaxis–haptotaxis mechanisms in cancer invasion: A multiscale derivation and computational perspective

Abdelghafour Atlas[1], Mostafa Bendahmane[2,*], Fahd Karami[3], Jacques Tagoudjeu[4] and Mohamed Zagour[5]

[1] Ecole Nationale des Sciences Appliquées de Marrakech, Université Cadi Ayyad, B.P. 575 Marrakech, Maroc

[2] Institut de Mathématiques de Bordeaux, Université de Bordeaux, Bordeaux Cedex, France

[3] École Supérieure de Technologie d'Essaouira, Université Cadi Ayyad, Essaouira El Jadida, Essaouira, Maroc

[4] École Nationale Supérieure Polytechnique de Yaoundé, Universite de Yaoundé I, Yaoundé, Cameroun

[5] Euromed University of Fes, UEMF, Morocco

* **Correspondence:** Email: mostafa.bendahmane@u-bordeaux.fr.

Abstract: This paper deals with the multiscale derivation of a nonlinear stochastic chemotaxis–haptotaxis system of cancerous tissue invasion from a new stochastic kinetic theory model based on the micro–macro decomposition technique. We show that this approach technically can lead to some systems known in the literature, such as the filling volume effect, and a new system by taking the stochasticity effect and nonlocal diffusion into account. We develop an asymptotic–preserving numerical scheme to solve the obtained equivalent micro–macro formulation numerically. The objective is to provide a uniformly stable scheme regarding the small parameters and consistency with the diffusion limit. Various numerical examples validate the proposed approach. Finally, we provide numerical simulations in the two-dimensional setting obtained by the macroscopic stochastic model.

Keywords: disease prevention; public health; kinetic theory; stochastic chemotaxis–haptotaxis system; cell biology; asymptotic–preserving scheme; numerical method

1. Introduction

Background

Cancer growth is a complicated multiscale phenomenon involving many inter-related biochemical and cellular processes at many different spatial and temporal scales [1]. It is a critical societal and scientific problem. Indeed, it is a large group of diseases that can affect any part of the body, characterized by abnormal cell proliferation and an increasing migration rate that can lead to invasion and organ spreading. As it is known, the biological experiments needed to test such hypotheses can be time-consuming and expensive with the currently available technology. Thus, mathematical modeling plays a primary role, giving an independent check of the consistency of the chosen hypothesis. Moreover, it can improve the experimental design by stating the measurements needed to test a particular theory (see [2]). At this point, mathematical modeling is a necessity that may be calibrated by experimental data. Furthermore, the significance and functions of variables representing specific biological features can be easily tested by testing the parameter values of descriptive equations. To achieve these purposes, a variety of mathematical models have been proposed in the literature for various aspects of cancer invasion of tissue extracellular matrix which focuses on the role of the plasminogen activation system, see [3–6]. For instance, the authors in [7] used reaction–diffusion equations to describe the interaction between the density of normal cells, tumor cells and the concentration of H^+–ions produced by the latter. Precisely, they assumed that cancer cells up-regulate certain mechanisms, which permit the extrusion of excessive protons and thus acidify the environment. Next, the authors of [8] proposed a population-based micro–macro model for acid-mediated tumor invasion restricted to the interactions between the microscopic dynamics of intracellular protons and their exchange with extracellular counterparts. While in [9], the authors proposed continuum micro–macro models explicitly accounting for sub-cellular events in the context of cancer cell migration. For comprehensive reviews of the modeling in this area, see [4, 10–13]. The theoretical studies on various models of cancer invasion are mathematically interesting [14–18]. We note that the system under consideration contains a strong coupling of reaction–diffusion equations and an ordinary differential equation (ODE). A considerable difficulty for mathematical analysis comes from the fact that ODE corresponds to a full degenerate reaction–diffusion equation and has no regularizing effect. However, the proof of the global existence and boundedness of solutions can be found in [9, 19, 20]. For the numerical studies, a number of numerical methods have been proposed in the literature. We refer the reader to the finite difference method [4, 5], the finite volume method [21], and the method of lines [1], which are the most commonly used methods in the literature for cancer migration models, and discontinuous Galerkin finite element methods have also been successfully applied in [22–24].

Deterministic system

The well-known tumor-induced angiogenesis has been established with the work by [25], where the authors proposed a simple model of tumor angiogenesis to describe experiments of tumor cells which resulted in the growth and migration of new blood vessels from the corneal limbus to the tumor [2]. However, several mathematical models have focused on the way in which tumor angiogenic factor (TAF) initiates and coordinates capillary growth [12]. The dimensionless governing equations can be

written as follows:

$$\begin{cases} \partial_t n = \underbrace{\operatorname{div}\left(D_n(n)\nabla n\right)}_{diffusion} - \underbrace{\operatorname{div}\left(\xi(m)\, n\nabla m\right)}_{chemotaxis} - \underbrace{\operatorname{div}\left(\chi(S)\, n\nabla S\right)}_{haptotaxis} + \underbrace{\mu_1\, n(1-n-S)}_{proliferation}, & x \in \Omega,\ t > 0, \\ \gamma\partial_t m = \underbrace{D_m\Delta m}_{diffusion} + \underbrace{\alpha n}_{production} - \underbrace{\beta m}_{decay}, & x \in \Omega,\ t > 0, \\ \partial_t S = -\underbrace{\delta m S}_{proteolysis} + \underbrace{\mu_2 S(1-n-S)}_{re-establishment}, & x \in \Omega,\ t > 0, \end{cases} \tag{1.1}$$

Table 1. Description of dimensionless variables and parameters.

Symbol	Description
n	Cancer cells density
m	The urokinase plasminogen activator concentration (uPA)
S	The extracellular matrix concentration (ECM)
D_n	Nonlinear diffusion of n
D_m	Diffusion coefficient of m
ξ	The sensitivity of chemotaxis
χ	The of sensitivity haptotaxis
μ_1	Cell proliferation rate
μ_2	ECM re-establishment rate
σ_i	Noise amplitude function
W_t^i	Cylindrical Wiener process
α	uPA production rate
β	uPA decay rate
δ	ECM degradation rate

where $\Omega \subset \mathbb{R}^N,\ N \geq 0$ is an open and bounded domain with a smooth boundary $\partial\Omega$; n and m represent the density of cancer cells and the urokinase plasminogen activator concentration, respectively; while S describes the concentration of the extracellular matrix (ECM). The functions $\xi(m)$ and $\chi(S)$ measure the sensitivity of chemotaxis and haptotaxis, respectively. The reaction term $\mu_1 n(1-n-S)$ assumes that in the absence of the ECM, cancer cell proliferation satisfies a logistic law, and $\mu_2 > 0$ embodies the ability of the ECM to remodel back to a normal level. Note that the parameter γ may take on the value of 0 or 1. Indeed, if $\gamma = 0$, this makes the simplifying assumption that the diffusion rate of the uPA is much greater than that of cancer cells (see [5]). Finally, the parameters α, β, and δ given in Table 1 are assumed to be positives. Observe that the term D_n is taken in the general form, and one may take it to be constant, nonlinear, or nonlocal. The last choice (with nonlocal diffusion) leads to a new mathematical model of the phenomenon of angiogenesis. Note that in the system (1.1), we consider cancer cell proliferation in which we get the logistic growth in the absence of S with a constant rate μ_1. However, it is interesting to integrate oscillatory behavior into the proliferation term of cancer cells and the ECM by considering function rates rather than constant rates. This has overcome a certain

weakness of continuum models, which generally only consider constant reproduction terms for cancer cells. In addition, it is also important to extend our model to include other interactions with other cell populations such as the urokinase receptor, matrix-like protein vitronectin and plasminogen activator inhibitors [4], stem cells, and effectors cell, tumor cells, as well as chemotherapy drugs [26].

Stochastic system

The deterministic systems above have some limitations, since biological systems are subject to environmental fluctuations [27]. Therefore, the explicit incorporation of stochasticity can fundamentally change and renormalize the behavior of a system of interacting species. Indeed, environmental fluctuations are essential components of an ecosystem. These fluctuations, rather than being deterministic, are stochastic. Since deterministic models do not consider environmental noise fluctuations, they have some limitations from a biological point of view [28]. Most natural phenomena do not follow strictly deterministic laws but rather oscillate randomly about some average value, so the deterministic equilibrium is no longer an absolutely fixed state with the advance of time [29]. The aforementioned fluctuations can be modeled by incorporating additive and multiplicative noise sources into the deterministic system. In this context, the present paper proposes a nonlinear stochastic chemotaxis–haptotaxis system. The system consists of three dimensionless reaction–diffusion stochastic partial differential equations describing the interactions of the endothelial cells, tumor angiogenic factor, and fibronectin with noise as follows:

$$\begin{cases} dn = \underbrace{\operatorname{div}\left(D_n(n)\nabla n\right)\mathrm{d}t}_{diffusion} - \underbrace{\operatorname{div}\left(\xi(m)\, n\nabla m\right)\mathrm{d}t}_{chemotaxis} - \underbrace{\operatorname{div}\left(\chi(S)\, n\nabla S\right)\mathrm{d}t}_{haptotaxis} \\ \qquad\qquad + \underbrace{\mu_1\, n(1-n-S)\,\mathrm{d}t}_{proliferation} + \underbrace{\sigma_1(n)dW_t^1}_{noise}, \\ \gamma dm = \underbrace{D_m\Delta m\,\mathrm{d}t}_{diffusion} + \underbrace{\alpha n\,\mathrm{d}t}_{production} - \underbrace{\beta m\,\mathrm{d}t}_{decay} + \gamma\,\underbrace{\sigma_2(m)dW_t^2}_{noise}, \\ dS = -\underbrace{\delta m S\,\mathrm{d}t}_{proteolysis} + \underbrace{\mu_2 S(1-n-S)\,\mathrm{d}t}_{re-establishment} + \underbrace{\sigma_3(S)dW_t^3}_{noise}. \end{cases} \tag{1.2}$$

In $\Omega_T = \Omega \times (0,T)$, $T > 0$ is a fixed time. In the system (1.2), W_t^i is a cylindrical Wiener process, with the noise amplitude function σ_i verifying $\sigma_i(0) = 0$ for $i = 1,2,3$. Formally, we can think of $\sigma_i(w)\, dW_t^i$ as $\sum_{k\geq 1} \sigma_{k,w}(w)\, dW_{k,w}(t)$, where $\{W_{k,w}\}_{k\geq 1}$ is a sequence of independent one-dimensional (1D) Brownian motions and $\{\sigma_{k,w}\}_{k\geq 1}$ is a sequence of noise coefficients. Note that the noise dW_t^i represents the independent environmental variables. Moreover, $\sigma_i(w)dW_t^i$ models random perturbations of the stochastic system (1.2). We consider a complete probability space $(\Omega, \mathcal{F}, P)$, along with a complete right-continuous filtration $\{\mathcal{F}_t\}_{t\in[0,T]}$ (we assume that the σ-algebra $\mathcal{F}$ is countably generated). Equipped with the Borel σ-algebra $\mathcal{B}(\mathbb{B})$, we let $\mathbb{B}$ be a separable Banach space. A $\mathbb{B}$-valued random variable X is a measurable mapping from $(\Omega, \mathcal{F}, P)$ to $(\mathbb{B}, \mathcal{B}(\mathbb{B}))$, $\Omega \ni \omega \mapsto X(\omega) \in \mathbb{B}$. A stochastic process $X = \{X(t)\}_{t\in[0,T]}$ is a collection of $\mathbb{B}$-valued random variables $X(t)$. The stochastic process X is *measurable* if the map $X : D \times [0,T] \to \mathbb{B}$ is measurable from $\mathcal{F} \times \mathcal{B}([0,T])$ to $\mathcal{B}(\mathbb{B})$. The paths $t \to X(\omega, t)$ of a measurable process X are automatically Borel

measurable functions. A stochastic process X is *adapted* if $X(t)$ is $\mathcal{F}_t$ measurable for all $t \in [0, T]$. We refer to

$$\mathcal{S} = \left(\Omega, \mathcal{F}, \{\mathcal{F}_t\}_{t\in[0,T]}, P, \{W_k\}_{k=1}^{\infty}\right) \tag{1.3}$$

as a (Brownian) stochastic basis, where $\{W_k\}_{k=1}^{\infty}$ is a sequence of independent 1D Brownian motions adapted to the filtration $\{\mathcal{F}_t\}_{t\in[0,T]}$. Let the Hilbert space $\mathcal{U}$ be equipped with a complete orthonormal basis $\{\psi_k\}_{k\geq 1}$. We define the cylindrical Brownian motions W on $\mathcal{U}$ by $W := \sum_{k\geq 1} W_k\psi_k$. The vector space of all bounded linear operators from $\mathcal{U}$ to $\mathbb{X}$ is denoted $L(\mathcal{U}, \mathbb{X})$, where $\mathbb{X}$ is a separable Hilbert space with the inner product $(\cdot,\cdot)_{\mathbb{X}}$ and norm $\|\cdot\|_{\mathbb{X}}$. We use $L_2(\mathcal{U}, \mathbb{X})$ to denote the collection of Hilbert–Schmidt operators from $\mathcal{U}$ to $\mathbb{X}$. Note that, for the stochastic model (1.2), a natural choice is $\mathbb{X} = L^2(D)$. In this paper, the stochastic process (for $i = 1, 2, 3$)

$$W_i(\omega, t, \cdot) := \sum_{k\geq 1} W_{i,k}(\omega, t)\psi_k(\cdot) \tag{1.4}$$

is referred to as a cylindrical Brownian motion evolving over $\mathcal{U}$. The right-hand side of (1.4) converges on the Hilbert space $\mathcal{U}_0$, with the embedding $\mathcal{U} \subset \mathcal{U}_0$ being Hilbert–Schmidt. Via standard martingale arguments, W_i is almost surely continuous with values in $\mathcal{U}_0$, i.e., $W_i(\omega, \cdot, \cdot)$ belongs to $C([0, T]; \mathcal{U}_0)$ for P almost everywhere $\omega \in D$, and also $L^2(D, \mathcal{F}, P; C([0, T]; \mathcal{U}_0))$. Without loss of generality, we assume that the filtration $\{\mathcal{F}_t\}_{t\in[0,T]}$ is generated by W_i and the initial condition for $i = 1, 2, 3$. For a given a cylindrical Brownian motion W_i, we can define the Itô stochastic integral $\int \sigma_i\, dW_i$ as follows (e.g., [30, 31]) for $i = 1, 2, 3$

$$\int_0^t \sigma_i\, dW_i = \sum_{k=1}^{\infty} \int_0^t \sigma_{i,k}\, dW_{i,k}, \qquad \sigma_{i,k} := \sigma_i\psi_k, \tag{1.5}$$

where σ_i is a predictable X-valued process satisfying

$$\sigma_i \in L^2\Big(\Omega, \mathcal{F}, P; L^2((0, T); L_2(\mathcal{U}, \mathbb{X}))\Big).$$

We impose conditions on the noise σ_i. For each $u_i \in L^2(D)$, we assume that $\sigma_i(u_i) : \mathcal{U} \to L^2(D)$ is defined by

$$\sigma_i(u_i)\psi_k = \sigma_{i,k}(u_i(\cdot)), \quad k \geq 1, \qquad \text{for } i = 1, 2, 3$$

for some real-valued functions $\sigma_{i,k}(\cdot,\cdot) : \mathbb{R}^2 \to \mathbb{R}$ that satisfy (for $i = 1, 2, 3$)

$$\begin{aligned} &\sum_{k\geq 1} \left|\sigma_{i,k}(u_i)\right|^2 \leq C_\sigma(1 + |u_i|^2), \\ &\sum_{k\geq 1} \left|\sigma_{i,k}(\bar{u}_i) - \sigma_{i,k}(\hat{u}_i)\right|^2 \leq C_\sigma(|\bar{u}_i - \hat{u}_i|^2), \end{aligned} \tag{1.6}$$

$\forall u_i, \bar{u}_i, \hat{u}_i \in \mathbb{R}$, for a constant $C_\sigma > 0$. Consequently,

$$\begin{aligned} &\|\sigma_i(u_i)\|^2_{L_2(\mathcal{U},L^2(\Omega))} \leq C_\sigma\left(1 + \|u_i\|^2_{L^2(D)}\right), \\ &\|\sigma_i(\bar{u}_i) - \sigma_i(\hat{u}_i)\|^2_{L_2(\mathcal{U},L^2(\Omega))} \leq C_\sigma\Big(\|\bar{u}_i - \hat{u}_i\|^2_{L^2(D)}\Big), \end{aligned} \tag{1.7}$$

where $u_1 = n$, $u_2 = m$, and $u_3 = S$.
System (1.2) is complemented with the following boundary conditions in $\Sigma_T := (0, T) \times \partial\Omega$ and the initial data

$$\begin{aligned} &(- D_n(n)\nabla n + \chi(m)\, n\nabla m + \xi(S)\, n\nabla S) \cdot \eta = 0, \quad D_m \nabla m \cdot \eta = 0, \qquad (t, x) \in \Sigma_T, \\ &n(0, x) = n_0(x), \quad m(0, x) = m_0(x), \quad S(0, x) = S_0(x), \qquad x \in \Omega, \end{aligned} \tag{1.8}$$

where η is the unit outward normal to Ω on $\partial\Omega$.

Note that we used multiplicative noise to incorporate the uncertainty and variability inherent in cancer progression into the mathematical model. The inclusion of this multiplicative noise is justified by biological and mathematical arguments; see [32]. Biologically, tumor progression is driven by highly variable and state-dependent processes, including cell proliferation and interaction with the ECM, all influenced by local cell density, nutrient availability, and micro-environmental heterogeneity. These fluctuations are not uniform but intensify in regions of low or high tumor density, such as at the invasive front, where stochastic effects are most pronounced. Moreover, this noise naturally captures this state-dependent randomness by allowing its intensity to adapt to the local value of tumor cell density or associated variables.

In this paper, we are interested with the multiscale derivation of a nonlinear stochastic chemotaxis–haptotaxis system (1.2) P^0 of cancer invasion of tissue using a new stochastic kinetic theory model P^ε according to the micro–macro decomposition method as shown in Figure 1. Note that the main idea of this method consists in rewriting the kinetic model, as coupled system of a microscopic part and a macroscopic one. Indeed, the distribution function is decomposed into its corresponding equilibrium and the deviation. Many works adopted this technique within different fields of application, such as chemotaxis phenomena [14, 33–35], the formation of patterns induced by cross-diffusion [36, 37], and angiogenesis phenomena [14, 38]; for more details, we refer to a recent review [39]. We note that the micro–macro decomposition method has been used to design a numerical scheme P_h^ε that preserves the asymptotic property in the limit P_h^0 introduced by [40, 41]; in other words, a stable numerical scheme in the limit along the transition from kinetic to macroscopic regimes. This approach was generalized for a variety of kinetic models; see, for example, [42–44]. This concept is a very challenging task because it is so expensive in terms of time due to the singularity in the kinetic model. The difficulty increased with the presence of stochastic terms in the studied model. For this reason, it is recommended to reformulate this singularity into an equivalent micro–macro formulation that is a regular perturbation of the derivation model; for more details, see [33, 36, 37, 45]. Compared with the existing works, in this paper we derive a cancer angiogenesis model (1.2) according to the micro–macro decomposition method, considering a more general random modification of the direction of the cells, and the stochastic terms are considered. Additionally, we develop an asymptotic–preserving numerical scheme which is stable and convergent in the limit along the transition from stochastic kinetic to hydrodynamic regimes. Note that the adopted multiscale derivation approach enables a deeper understanding of the specific characteristics of the kinetic and macroscopic regimes. Indeed, on the one hand, thanks to the proposed kinetic theoretical system, we obtain more detailed information on the density of cancer cells, the concentration of urokinase plasminogen activator, and the concentration of the extracellular matrix, as well as on their velocities. On the other hand, we predict their spatio-temporal dynamics via the

macroscopic system. We note that the authors in [46] propose an innovative modeling framework for cell migration within anisotropic environments characterized by biochemical heterogeneity and interspecies interactions, using glioma invasion in brain tissue as a representative case study influenced by hypoxia-induced angiogenesis. Their multiscale approach provides a connection between single-cell and mesoscopic dynamics and the emergent population-level behavior, culminating, at the macroscopic scale, in a flux-limited glioma diffusion model incorporating multiple taxis mechanisms.

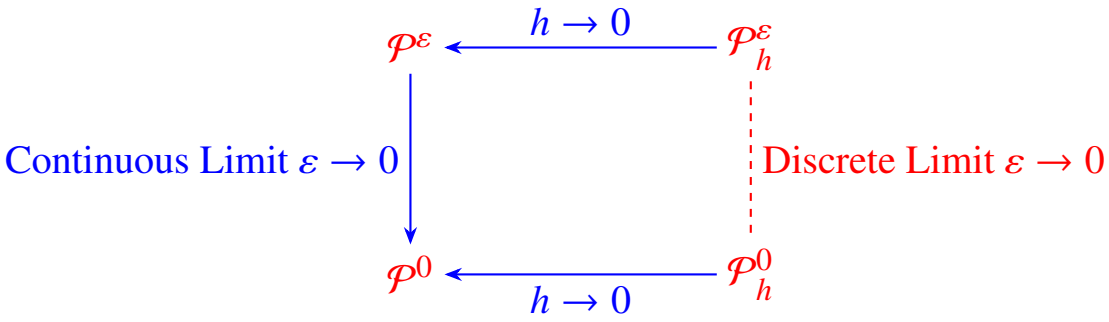

Figure 1. Schematic diagram of the multiscale framework.

This paper is organized as follows: In Section 2, we present the stochastic kinetic theory model and its properties. An equivalent system of the model (2.1) is obtained according to the multiscale approach. In addition, we derive a general macroscopic chemotaxis–haptotaxis system. This section is closed by setting some applications, specifically stochastic systems with linear, nonlinear, and nonlocal diffusion. Section 3 is devoted to developing a numerical method for the solution of the stochastic kinetic theory model. We present various numerical tests where the aim is to show the asymptotic–preserving scheme property and to depict some cancer invasion phenomena. Finally, in Section 4, we provide some numerical simulations obtained from the macroscopic model in the two-dimensional (2D) setting.

2. Multiscale derivation of the stochastic chemotaxis–haptotaxis system

This section deals with the derivation of the nonlinear stochastic chemotaxis–haptotaxis system (1.2) via an improved stochastic kinetic theory model. After a short presentation of the properties of the kinetic model, we give the equivalent micro–macro formulation according to the micro–macro decomposition method. Next, we derive a class of general macroscopic systems describing the angiogenesis phenomena. Finally, we show that this present approach technically can lead to some systems known in the literature such as the filling volume effect, as well as a new system by taking the stochasticity effect and nonlocal diffusion into account.

2.1. Stochastic kinetic theory model

Here, we state our stochastic kinetic theory model and we present its properties. The ultimate objective is to derive the macroscopic chemotaxis–haptotaxis system (1.2) from the following

stochastic kinetic theory model according the parabolic–parabolic scale [14]

$$\begin{cases} \varepsilon df + v \cdot \nabla_x \mathcal{F}(f)\, dt = \dfrac{1}{\varepsilon}\mathcal{L}(f, g_1, g_2)\, dt + H(f, g_1, g_2)\, dt + \varepsilon\sigma_1(f) dW_t^1, \\ \gamma\, dg_1 = \Big(D_1 \Delta g_1 + \alpha \displaystyle\int_V f\, dv - \beta g_1\Big) dt + \gamma\sigma_2(g_1) dW_t^2, \\ dg_2 = -\delta g_1 g_2\, dt + \mu_2 g_2\Big(1 - \displaystyle\int_V f\, dv\ - g_2\Big) dt + \sigma_3(g_2) dW_t^3, \\ f(0, x, v) = f_0(x, v), \qquad g_1(0, x) = g_{1,0}(x), \qquad g_2(0, x) = g_{2,0}(x), \end{cases} \tag{2.1}$$

where $f = f(t, x, v)$ is a generalized distribution function depending on the time t, the position $x \in \Omega \subset \mathbb{R}^d$, and the velocity $v \in V \subset \mathbb{R}^d$, where V is a symmetric domain that describes the statistical distribution of epithelial cells. The nonlocal function F is defined by

$$\mathcal{F}(f)(t, x, v) = \phi\Big(\int_\Omega \int_V f(t, x, v) dv dx\Big) f(t, x, v).$$

The operator $\mathcal{L}$ models a random modification of the direction of the cells and ε is a positive constant parameter. It assumed that the linear operator $\mathcal{L}$ admits the following decomposition:

$$\mathcal{L}(f, g_1, g_2) = \mathcal{T}_0(f) + \varepsilon \sum_{i=1}^{2} \mathcal{T}_i(g_i)(f),$$

where the operators $\mathcal{T}_i$, which are linear with respect to f, and the integral operators are defined as follows [37]:

$$\mathcal{T}_i(g_i, f) = \int_V [T_i(g_i, v, v^*) f(t, x, v^*) - T_i(g_i, v^*, v) f(t, x, v)] dv^*,$$

for $i = 1, 2$, where $T_i(v, v^*)$ is the probability kernel over the new velocity $v \in V$, assuming that the previous velocity was v^*. Herein, we assume that

$$H(f, g_1, g_2) = \varepsilon f\, H_1\Big(\int_V f dv, g_1\Big), \tag{2.2}$$

where H_1 is independent of the velocity v. In the model (2.1), W_i is a cylindrical Wiener process, with the noise amplitude function σ_i for $i = 1, 2$. Formally, we can think of $\sigma_i(f_i)\, dW_t^i$ as $\sum_{k\geq 1} \sigma_{k,i}(f_i)\, dW_t^{k,i}$, where $\{W^{k,i}\}_{k\geq 1}$ is a sequence of independent 1D Brownian motions and $\{G^{k,i}\}_{k\geq 1}$ is a sequence of noise coefficients. The noise dW^i represents the independent environmental variables, namely the time-dependent Gaussian white noise. Herein, the following assumptions are necessary to develop the micro–macro decomposition method.

Assumption (H1). a. The operators $\mathcal{T}_i$ preserve the local mass

$$\int_V \mathcal{T}_0(f) dv = \int_V \mathcal{T}_i(f, g_i) dv = 0, \quad g_i \geq 0, \quad i = 1, 2. \tag{2.3}$$

b. The operator $\mathcal{T}_0(f)$ is independent on g_i, $i = 1, 2$.

Assumption (H2). A bounded velocity distribution $M(v) > 0$ exists, independent of x and t, such that

1) The flow produced by the equilibrium distribution M vanishes, and M is normalized as

$$\int_V vM(v)dv = 0, \quad \int_V M(v)dv = 1. \tag{2.4}$$

2) The detailed balance

$$T_0(v^*, v)M(v) = T_0(v, v^*)M(v^*)$$

holds.

3) The kernels $T_0(v, v^*)$ is bounded, and a constant $\sigma > 0$ exists such that

$$T_0(v, v^*) \geq \kappa M(v) \tag{2.5}$$

for all $(v, v^*) \in V \times V$, $x \in \mathbb{R}^d$ and $t > 0$.

Using the same arguments as in [29], the following lemma states the necessary properties of the operator $\mathcal{T}_0$.

Lemma 2.1. *Suppose that the Assumptions (H1) and (H2) hold. We then have the following properties of the operator $\mathcal{T}_0$:*

1) *For $f \in L^2(V, \frac{dv}{M(v)})$, the equation $\mathcal{T}_0(g) = f$ has a unique solution g which satisfies*

$$\int_V g dv = 0 \quad \text{if and only if} \quad \int_V f dv = 0.$$

2) *The operator $\mathcal{T}_0$ is self-adjoint in the space $L^2(V, \frac{dv}{M(v)})$.*
3) *The equation $\mathcal{T}_0(g) = vM(v)$, has a unique solution called $\theta(v)$.*
4) *The kernel of $\mathcal{T}_0$ is $N(\mathcal{T}_0) = vect(M(v))$.*

2.2. micro–macro formulation

In this subsection, we show that the kinetic equation (2.1) can be equivalently written as a system coupling a hydrodynamic part with a kinetic part of the distribution function.

In what follows, the integral with respect to the variables v and u will be denoted $\langle . \rangle$, and let f be a solution of (2.1). We decompose f as follows: $f = M(v)n + \varepsilon h$, where $n = \int_V f dv =: \langle f \rangle$ is the mass density. Then, $\langle h \rangle = 0$, $\phi(\int_\Omega \langle f \rangle dx) = \phi(\int_\Omega n dx) := \phi(n)$ and one has

$$d(M(v)n) + \varepsilon dh + \frac{1}{\varepsilon} vM(v) \cdot \nabla_x(\phi(n)\, n)\ \mathrm{d}t + v \cdot \nabla_x(\phi(n)h)\ \mathrm{d}t = \frac{1}{\varepsilon}\mathcal{T}_0(h)\ \mathrm{d}t \tag{2.6}$$

$$+\frac{1}{\varepsilon}\sum_{i=1}^{2} \mathcal{T}_i(g_i)(M(v)n)\ \mathrm{d}t + \sum_{i=1}^{2} \mathcal{T}_i(g_i)(h)\ \mathrm{d}t + M(v)nH_1\ \mathrm{d}t + \varepsilon h H_1\ \mathrm{d}t + \sigma_1(n)dW_t^1.$$

We now use a projection technique to separate the macroscopic and microscopic quantities $n(t, x)$ and $h(t, x, v)$.

Let P_M denotes the orthogonal projection onto $N(\mathcal{T}_0)$. Then

$$P_M(h) = \langle h \rangle M(v), \quad \text{for any} \quad h \in L^2(V, \frac{dv}{M(v)}).$$

Lemma 2.2. *One has the following properties for the projection P_M:*

$$(I - P_M)(M(v)n) = P_M(h) = 0,$$
$$(I - P_M)(vM(v) \cdot \nabla_x(\phi(n)\, n)) = vM(v) \cdot \nabla_x(\phi(n)\, n),$$
$$(I - P_M)(\mathcal{T}_i(g_i)(M(v)n) = \mathcal{T}_i(g_i)(M(v)n), \quad i = 1, 2,$$
$$(I - P_M)(\mathcal{T}_i(g_i)(h) = \mathcal{T}_i(g_i)(h), \quad i = 1, 2.$$

Taking the operator $I - P_M$ in Eq (2.6) and using Lemma 2.2 above, yields

$$\varepsilon dh + \frac{1}{\varepsilon} vM(v) \cdot \nabla_x(\phi(n)\, n)\, \mathrm{d}t + (I - P_M)(v \cdot \nabla_x(\phi(n)\, h))\, \mathrm{d}t = \frac{1}{\varepsilon}\mathcal{T}_0(h)\, \mathrm{d}t$$
$$+\frac{1}{\varepsilon}\sum_{i=1}^{2} \mathcal{T}_i(g_i)(M(v)n)\, \mathrm{d}t + \sum_{i=1}^{2} \mathcal{T}_i(g_i)(h) + \varepsilon h H_1\, \mathrm{d}t + (I - P_M)\sigma_1(n) dW_t^1, \tag{2.7}$$

Integrating (2.6) over v and using Assumptions *(*H1) and *(*H2), yields:

$$dn + \phi(n) \langle v \cdot \nabla_x h \rangle\, \mathrm{d}t = nH_1\, \mathrm{d}t + \Big\langle \sigma_1(n) \Big\rangle dW_t^1. \tag{2.8}$$

Then, the micro–macro formulation finally reads

$$\begin{cases} \varepsilon dh + \dfrac{1}{\varepsilon} vM(v) \cdot \nabla_x(\phi(n)\, n)\, \mathrm{d}t + (I - P_M)(v \cdot \nabla_x(\phi(n)\, h))\, \mathrm{d}t = \dfrac{1}{\varepsilon}\mathcal{T}_0(h)\, \mathrm{d}t \\ \qquad\qquad +\dfrac{1}{\varepsilon}\displaystyle\sum_{i=1}^{2} \mathcal{T}_i(g_i)(M(v)n)\, \mathrm{d}t + \sum_{i=1}^{2} \mathcal{T}_i(g_i)(h)\, \mathrm{d}t + \varepsilon h H_1\, \mathrm{d}t + (I - P_M)\sigma_1(n) dW_t^1, \\ dn + \phi(n) \langle v \cdot \nabla_x h \rangle\, \mathrm{d}t = nH_1\, \mathrm{d}t + \sigma_1(n) dW_t^1, \\ \gamma dg_1 = D_1 \Delta g_1\, \mathrm{d}t + \alpha n\, \mathrm{d}t - \beta g_1\, \mathrm{d}t + \gamma \sigma_2(g_1) dW_t^2, \\ dg_2 = -\delta g_1 g_2\, \mathrm{d}t + \mu_2 g_2\Big(1 - n - g_2\Big)\, \mathrm{d}t + \sigma_3(g_2) dW_t^3. \end{cases} \tag{2.9}$$

Equation (2.9) is the micro–macro formulation of the kinetic equation (2.1). The following proposition shows that this formulation is indeed equivalent to the stochastic kinetic theory model (2.1).

Proposition 2.1. *i) Let f be a solution of the kinetic equation (2.1). Then the functions (n, h), where $n = \langle f \rangle$ and $h = \dfrac{1}{\varepsilon}(f - Mn)$ is a solution to a coupled system (2.9) with the associated initial data.*

$$n(t = 0) = n_0 = \langle f_0 \rangle, \quad h(t = 0) = h_0 = \frac{1}{\varepsilon}(f_0 - Mn_0). \tag{2.10}$$

ii) Conversely, if (n, h) satisfies the system (2.9) with the initial data (n_0, h_0) such that $\langle h_0 \rangle = 0$, then $f = Mn + \varepsilon h$, is a solution to kinetic model (2.1) with the initial data $f_0 = Mn_0 + \varepsilon h_0$, and we have $n = \langle f \rangle$ and $\langle h \rangle = 0$.

2.3. Derivation of a general macroscopic systems

Here, we briefly show that the micro–macro formulation (2.9) of the kinetic equation (2.1) allows to very easily obtain the corresponding macroscopic models as ε goes to 0, without using the Hilbert expansion. Indeed, Eq (2.9) gives

$$\mathcal{T}_0(h) = vM(v) \cdot \nabla_x n - \sum_{i=1}^{2} \mathcal{T}_i(g_i)(M(v)n) + O(\varepsilon),$$

and as

$$\langle vM(v) \rangle = \langle \sum_{i=1}^{2} \mathcal{T}_i(g_i)(M(v)n) \rangle = 0.$$

It implies that the operator $\mathcal{T}_0$ is invertible, and one obtains

$$h = \mathcal{T}_0^{-1}\Big(vM(v) \cdot \nabla_x(\phi(n)\, n) - \sum_{i=1}^{2} \mathcal{T}_i(g_i)(M(v)n) \Big) + O(\varepsilon). \tag{2.11}$$

Using (2.8) and inserting (2.11) into (2.9), yields the following macroscopic models:

$$\begin{cases} dn + \operatorname{div}\Big(\sum_{i=1}^{2} \rho(n)\alpha_i(g_i) - \psi(n) \cdot \nabla n \Big)\, \mathrm{d}t = nH_1\, \mathrm{d}t + \sigma_1(n) dW_t^1 + O(\varepsilon), \\ \gamma dg_1 = D_1 \Delta g_1\, \mathrm{d}t + \alpha n\, \mathrm{d}t - \beta g_1\, \mathrm{d}t + \gamma \sigma_2(g_1) dW_t^2, \\ dg_2 = -\delta g_1 g_2\, \mathrm{d}t + \mu_2 g_2\Big(1 - n - g_2\Big)\, \mathrm{d}t + \sigma_3(g_2) dW_t^3, \end{cases} \tag{2.12}$$

where ρ, ψ, and $\alpha_i(g_i)$ are given by

$$\rho(n) = \phi(n)\, n, \tag{2.13}$$

$$\psi(n) = -\phi(n)^2 \int_V v \otimes \theta(v) dv\,, \tag{2.14}$$

$$\alpha_1(g_1) = -\int_V \frac{\theta(v)}{M(v)} \mathcal{T}_1(g_1)[M(v)] dv, \tag{2.15}$$

$$\alpha_2(g_2) = -\int_V \frac{\theta(v)}{M(v)} \mathcal{T}_2(g_2)[M(v)] dv\,. \tag{2.16}$$

2.4. Applications

We consider the case where the set for velocity is a sphere of radius $r > 0$, $V = rS^{d-1}$. It can be shown that for a particular choice of $T_i(g_i, v, v^*)$ $i = 0, 1, 2$, the model (2.1) is asymptotic to the system (1.2). Precisely, we consider, in (2.1), a particular choice of terms

$$g_1 = m, \quad g_2 = S, \qquad H_1(n, S) = \mu_1(1 - n - S).$$

We assume that the kernel T_0 is given by

$$T_0 = \sigma M(v), \qquad \sigma > 0.$$

Then $\mathcal{T}_0(f)$ is a relaxation operator

$$\mathcal{T}_0(f) = \kappa\Big(M(v)\langle f\rangle - f\Big). \tag{2.17}$$

Using (2.4), (2.17), and Lemma 2.2, then the θ solution of $\mathcal{T}_0(\theta(v)) = vM(v)$ is given by $\theta(v) = -\dfrac{1}{\sigma}vM(v)$.

Example 1: Derivation of the stochastic chemotaxis–haptotaxis system. In this example, we derive the system where the diffusion is assumed to be constant as well the functions ξ and χ, i.e., $D_n(n) = D_1$, $\xi(m) = \xi_m$, and $\chi(S) = \chi_S$. Consequently, we rewrite the system (1.2) as follows:

$$\begin{cases} dn = D_1\Delta n\,\mathrm{d}t - \operatorname{div}(\xi_m\, n\nabla m)\,\mathrm{d}t - \operatorname{div}(\chi_S\, n\nabla S)\,\mathrm{d}t + \mu_1\, n(1-n-S)\,\mathrm{d}t + \sigma_1(n)dW_t^1, \\ \gamma dm = D_m\Delta m\,\mathrm{d}t + \alpha n\,\mathrm{d}t - \beta m\,\mathrm{d}t + \gamma\sigma_2(m)dW_t^2, \\ dS = -\delta mS\,\mathrm{d}t + \mu_2 S(1-n-S)\,\mathrm{d}t + \sigma_3(S)dW_t^3. \end{cases} \tag{2.18}$$

First, let the function $\phi = 1$. Then from Eq (2.14), we obtain

$$\psi(n) = -\int_V v\otimes\theta(v)dv := D_1.$$

Now, let $T_1[g_1]$ and $T_2[g_2]$ be given by

$$T_1[g_1] = \xi_0 M(v)v\cdot\nabla_x g_1, \quad T_2[g_2] = \chi_0 M(v)v\cdot\nabla_x g_2,$$

then

$$\mathcal{T}_1[g_1](M) = \xi_0 M(v)v\cdot\nabla_x g_1 \text{ and } \mathcal{T}_2[g_2](M) = \chi_0 M(v)v\cdot\nabla_x g_2.$$

Therefore, using Eqs (2.15) and (2.16), one has

$$\alpha_1(g_1) = \frac{\xi_0}{\sigma}\int_V v\otimes vM(v)dv\ \ \nabla_x g_1, \text{ and } \alpha_2(g_2) = \frac{\chi_0}{\sigma}\int_V v\otimes vM(v)dv\,\nabla_x g_2.$$

Finally, we take

$$\xi_m = \frac{\xi_0}{\sigma}\int_V v\otimes vM(v)dv \quad \textit{and} \quad \chi_S = \frac{\chi_0}{\sigma}\int_V v\otimes vM(v)dv \tag{2.19}$$

to obtain the macroscopic chemotaxis–haptotaxis system (2.18).

Example 2: Derivation of the nonlinear diffusion stochastic chemotaxis–haptotaxis system with a filling volume effect. We deal with the derivation of the nonlinear system where the functions ξ and χ are given by $\xi(m) = \xi_m$ and $\chi(S) = \frac{k}{k+S}$ with $k > 0$. Consequently, we rewrite the system (1.2) as follows:

$$\begin{cases} dn = \operatorname{div}(D_2(n)\cdot\nabla n)\,\mathrm{d}t - \operatorname{div}(\xi_m n\nabla m)\,\mathrm{d}t - \operatorname{div}\Big(\dfrac{k\,n}{k+S}\nabla S\Big)\mathrm{d}t + \mu_1\, n(1-n-S)\,\mathrm{d}t + \sigma_1(n)dW_t^1, \\ \gamma dm = D_m\Delta m\,\mathrm{d}t + \alpha n\,\mathrm{d}t - \beta m\,\mathrm{d}t + \gamma\sigma_2(m)dW_t^2, \\ dS = -\delta mS\,\mathrm{d}t + \mu_2 S(1-n-S)\,\mathrm{d}t + \sigma_3(S)dW_t^3. \end{cases} \tag{2.20}$$

We consider the same choices as in Example 1 of ϕ and of $T_1[g_1]$, while the kernel $T_2[g_2]$ is now given by

$$T_2[g_2] = v\Big(\frac{\sigma}{n\langle v\times v\rangle}\Big(D_2(n)+D_n\Big)\cdot\nabla n + \frac{k\,M^2(v)}{r^2(k+g_2)}\cdot\nabla g_2\Big),$$

then

$$\mathcal{T}_2[g_2](M) = \frac{\kappa v}{n\,\langle v\times v\rangle}\Big(D_2(n)+D_n\Big)\cdot\nabla n + \frac{k\,M^2(v)}{r^2(k+g_2)}v\cdot\nabla g_2.$$

Therefore, using Eq (2.16) one has

$$\alpha_2(g_2) = \Big(D_2(n)+D_n\Big)\nabla n + \frac{k}{k+g_2}\nabla g_2.$$

Finally, we collect the obtained results and replace them in the system (2.12) to derive the system (2.20).

Example 3: Derivation of the nonlocal diffusion stochastic chemotaxis–haptotaxis system with a filling volume effect. Here, we derive a new system within a nonlocal diffusion under the filling volume effect. The proposed system is given as follows:

$$\begin{cases} dn = D_3\Big(\displaystyle\int_\Omega n\,dx\Big)\Delta n\,\mathrm{d}t - \mathrm{div}\,(\xi_m\, n\nabla m)\,\mathrm{d}t - \mathrm{div}\Big(\frac{k\,n}{k+S}\nabla S\Big)\mathrm{d}t \\ \qquad\qquad +\mu_1\, n(1-n-S)\,\mathrm{d}t + \sigma_1(n)dW_t^1, \\ \gamma dm = D_m\Delta m\,\mathrm{d}t + \alpha n\,\mathrm{d}t - \beta m\,\mathrm{d}t + \gamma\sigma_2(m)dW_t^2, \\ dS = -\delta m S\,\mathrm{d}t + \mu_2 S(1-n-S)\,\mathrm{d}t + \sigma_3(S)dW_t^3. \end{cases} \tag{2.21}$$

Let the function $\phi(s) = \sqrt{D_3(s)}$ where $s>0$, then from Eqs (2.13) and (2.14), we obtain

$$\rho(n) = \phi(n)\,n,\quad \psi(n) = D_3\Big(\int_\Omega n\,dx\Big)\int_V v\otimes\theta(v)dv\,.$$

The kernel operators T_1 and T_2 are given by

$$T_1[g_1] = \xi_0\frac{M(v)}{\phi(n)}v\cdot\nabla_x g_1 \text{ and } T_2[g_2] = \frac{k\,M^2(v)}{r^2(k+g_2)\phi(n)}v\cdot\nabla g_2,$$

then

$$\mathcal{T}_1[g_1](M) = \frac{\xi_0 M(v)}{\phi(n)}v\cdot\nabla_x g_1 \text{ and } \mathcal{T}_2[g_2](M) = \frac{k\,M^2(v)}{r^2(k+g_2)\phi(n)}v\cdot\nabla g_2.$$

Therefore, using Eq (2.16), one has

$$\alpha_1(g_1) = \frac{\xi_0}{\sigma\phi(n)}\int_V v\otimes vM(v)dv\ \ \nabla_x g_1,\ \text{and}\ \ \alpha_2(g_2) = \frac{k}{(k+g_2)\phi(n)}\nabla g_2.$$

Finally, we collect the obtained results and replace them in the system (2.12) to derive the system (2.21).

3. Numerical methods for stochastic kinetic model in 1D

In this section, we develop numerical methods for the solution of the stochastic kinetic model (2.1) using the micro–macro formulation (2.9) in 1D. The discretization is carried out with respect to each independent variable (time, space, and velocity). The well-known Euler–Maruyama scheme is used with an implicit–explicit (IMEX) strategy for the time discretization, while the spatial discretization is carried out by a finite volume scheme, and the velocity discretization is performed by a quadrature formula.

3.1. asymptotic–preserving scheme

This section aims to develop and to propose asymptotic–preserving (AP) numerical schemes in 1D space; in other words, the uniform stability with respect to the parameter ε and the consistency with the chemotaxis–haptotaxis limit. We assume the same activity for all the particles. Moreover, it is subjected to the following initial condition:

$$f(0, x, v) = f_0(x, v). \tag{3.1}$$

It is shown that kinetic equation (2.1) is equivalent to the system (2.9) which is implemented with the following initial conditions:

$$n(t = 0) = n_0 = \langle f_0 \rangle,\ h(t = 0) = h_0 = \frac{1}{\varepsilon}(f_0 - Mn_0),\ S(t = 0) = S_0,\ m(t = 0) = m_0. \tag{3.2}$$

The discretization of the problems (2.9), (3.1), and (3.2) is carried out with respect to each independent variable (time, velocity, and space).

3.1.1. Semi-implicit time discretization

In this first step, we present the time discretization of our coupled system. We use Δt to denote a fixed time step, and t_k to denote a discrete time such that $t_k = k\,\Delta t\ k \in \mathbb{N}$. The approximation of $n(t, x)$, $h(t, x, v)$, and $\phi(n)$ at the time step t_k are denoted, respectively, by $n^k \approx n(t_k, x)$, $h^k \approx h(t_k, x, v)$ and $\phi^k \approx \phi(t_k, x)$. In the first microscopic equation of (2.9), the only term which presents a stiffness in the collision part, for a small ε , is $\frac{1}{\varepsilon}\mathcal{T}_0(h)$. Hence we take an implicit scheme to ensure the stability for this term, while the other terms are still explicit, then one has

$$\begin{aligned} h^{k+1} + \Big(\frac{1}{\varepsilon^2}\phi^k v M(v)\cdot\nabla_x n^k + \frac{1}{\varepsilon}(I - P_M)(\phi^k v\cdot\nabla_x h^k)\Big)\Delta t = h^k\Big(+ \frac{1}{\varepsilon^2}\mathcal{T}_0(h^{k+1}) + \frac{1}{\varepsilon^2}\mathcal{T}_1(m^k)(M(v)n^k) \\ + \frac{1}{\varepsilon}\mathcal{T}_1(m^k)(h^k) + \frac{1}{\varepsilon^2}\mathcal{T}_2(S^k)(M(v)n^k) + \frac{1}{\varepsilon}\mathcal{T}_2(S^k)(h^k) + h^k H_1^k\Big)\Delta t + (I - P_M)\sigma_1(n^k)\Delta W_1^k, \end{aligned} \tag{3.3}$$

where

$$\Delta W_1^k = W_1^{k+1} - W_1^k = \sqrt{\Delta t}\,\delta_k^1$$

with δ_n^1 being independently and identically distributed (i.i.d.) random variables with a normal distribution. In the second macroscopic equation of (2.9), we take h at the time t_{k+1}, which gives

$$n^{k+1} = n^k - \phi^k\langle v\cdot\nabla_x h^{k+1}\rangle\Delta t + n^k H_1(n^k, S^k)\Delta t + \sigma_1(n^k)\Delta W_1^k. \tag{3.4}$$

Finally, replacing n in the third and the fourth equation by n^{k+1} one has

$$\gamma m^{k+1} = \gamma m^k + D_m \Delta m^{k+1} \Delta t + (\alpha n^{k+1} - \beta m^k)\Delta t + \gamma \sigma_2(m^k)\Delta W_2^k, \tag{3.5}$$

$$S^{k+1} = S^k - \delta m^{k+1} S^{k+1} \Delta t + \mu_2 S^k (1 - n^{k+1} - S^k)\Delta t + \sigma_3(S^k)\Delta W_3^k. \tag{3.6}$$

Proposition 3.1. *The time discretization (3.3) and (3.4) of the first and second equation of the system (2.9) is consistent with the first equation of (2.12) when ε goes to* 0.

3.1.2. Fully discrete 1D scheme

In this section, we construct a suitable space discretization of (3.3) and (3.5). The domain under consideration is $[0, L]$. The velocity space $[-V, V]$ can be treated by using a standard discretization. We define a staggered grid $x_i = i\,\Delta x$, $i = 0, \ldots, N_x$ with $N = \dfrac{L}{\Delta x}$, and the cell center points are $x_{i-\frac{1}{2}} = (i-\frac{1}{2})\Delta x$, $i = 0, \ldots, N_x+1$. Let n_i^k and $h_{i-\frac{1}{2}}^k$ be approximations of $n(t_k, x_i)$ and $h(t_k, x_{i-\frac{1}{2}}, v)$, respectively. The microscopic equation (3.3) is discretized at the points $x_{i+\frac{1}{2}}$, while the other macroscopic equations (3.4) and (3.5) are discretized at the points x_i. Then we obtain

$$\begin{aligned} h_{i+\frac{1}{2}}^{k+1} &+ \frac{1}{\varepsilon^2} v M(v) \phi^k \frac{n_{i+1}^k - n_i^k}{\Delta x}\Delta t + \frac{1}{\varepsilon}(I - P_M)(\phi^k v \cdot \nabla_x h_{i+\frac{1}{2}}^k)\Delta t = h_{i+\frac{1}{2}}^k + \frac{1}{\varepsilon^2}\mathcal{T}_0(h_{i+\frac{1}{2}}^{k+1})\Delta t \\ &+ \frac{1}{\varepsilon^2}\mathcal{T}_1(m_{i+\frac{1}{2}}^k)(M(v) n_{i+\frac{1}{2}}^k)\Delta t + \frac{1}{\varepsilon}\mathcal{T}_1(m_{i+\frac{1}{2}}^k)(h_{i+\frac{1}{2}}^k)\Delta t + \frac{1}{\varepsilon^2}\mathcal{T}_2(S_{i+\frac{1}{2}}^k)(M(v) n_{i+\frac{1}{2}}^k)\Delta t \\ &+ \tfrac{1}{\varepsilon}\mathcal{T}_2(S_{i+\frac{1}{2}}^k)(h_{i+\frac{1}{2}}^k)\Delta t + h_{i+\frac{1}{2}}^k H_1(n_{i+\frac{1}{2}}^k, S_{i+\frac{1}{2}}^k)\Delta t + (I - P_M)\sigma_1(n_{i+\frac{1}{2}}^k)\Delta W_1^k, \end{aligned} \tag{3.7}$$

$$n_i^{k+1} = n_i^k - \phi^k \Big\langle v \frac{h_{i+\frac{1}{2}}^{k+1} - h_{i-\frac{1}{2}}^{k+1}}{\Delta x} \Big\rangle \Delta t + n_i^k\, H_1(n_i^k, S_i^k)\Delta t + \sigma_1(n_i^k)\Delta W_1^k, \tag{3.8}$$

$$\gamma m_i^{k+1} = \gamma m_i^k + D_m \frac{m_{i+1}^{k+1} - 2m_i^{k+1} + m_{i-1}^{k+1}}{\Delta x^2}\Delta t + (\alpha n_i^{k+1} - \beta m_i^k)\Delta t + \gamma \sigma_2(m_i^k)\Delta W_2^k, \tag{3.9}$$

$$S_i^{k+1} = S_i^k + \delta_m m_i^{k+1} S_i^{k+1} \Delta t + \mu_2 S_i^k (1 - n_i^k - S_i^k)\Delta t + \sigma_3(S_i^k)\Delta W_3^k. \tag{3.10}$$

The velocity discretization is achieved by using the standard trapezoidal rule.

The spatial discretization error is $O(\max\{\Delta x^2, \varepsilon \Delta x\})$, since the spatial discretization error is $O(\Delta x)$ at the kinetic regime ($\varepsilon = O(1)$) and $O(\Delta x^2)$ at the diffusive limit (as $\varepsilon \to 0$). The Euler–Maruyama scheme yields the $O(\Delta t^{1/2})$ error for the temporal discretization, while the trapezoidal rule results in $O(\Delta v^2)$ accuracy for the velocity discretization, where Δv is the velocity step. Thus, the total error of the scheme is $O(\max\{\Delta x^2, \varepsilon \Delta x\}) + O(\Delta t^{1/2}) + O(\Delta v^2)$.

The scheme is conditionally stable. The time step size must satisfy the convection Courant-Friedrichs-Lewy (CFL) condition ($\Delta t = O(\Delta x)$) under the kinetic regime and the diffusion CFL condition ($\Delta t = O(\Delta x^2)$) at the diffusion limit. Additional time step restriction conditions, depending on the intensity of the multiplicative noise, may be required due the use of an explicit Euler–Maruyama scheme for the stochastic term. Strong multiplicative noise necessitates very small time steps to maintain stability and accuracy, resulting in a prohibitive computational cost for long-term simulations. Moreover, the Euler–Maruyama scheme lacks positivity-preserving property. The computational cost per time step is $O(N_x.N_v)$, where N_v is the total number of discrete velocities.

3.2. Numerical simulation

This subsection is devoted to presenting the numerical results in the case of 1D space. The ultimate aim is to validate the asymptotic–preserving scheme property, namely the uniform stability with respect to the parameter ε and consistent with the chemotaxis–haptotaxis limit. The computational domain in space is $[-1, 1]$, while the velocity space is $V = [-1, 1]$ with 64 discrete points which can be good enough for numerical simulations [47]. For all numerical simulations carried out below, we take the same dimensionless parameter values as in [5]; see Table 2.

Table 2. Dimensionless used parameters.

Symbol	Description	Value
D_n	Nonlinear diffusion of n	10^{-2}
D_m	Diffusion coefficient of m	10^{-2}
ξ	The sensitivity of chemotaxis	5×10^{-2}
χ	The sensitivity of haptotaxis	5×10^{-2}
μ_1	Cells proliferation rate	$\mu_1 = 0.005$
μ_2	ECM re-establishment rate	$\mu_2 = 0.1$
α	uPA production rate	0.05
β	uPA decay rate	0.3
δ	ECM degradation rate	10
γ	ECM degradation rate	1

The initial condition of tumor cells, the ECM, and the uPA protease density are given as

$$n(x, 0) = \exp(-100x^2), \qquad m(x, 0) = \frac{1}{2}\exp(-100x^2), \qquad S(x, 0) = 1 - \frac{1}{2}\exp(-100x^2),$$

and the initial cell distribution function is given by

$$f(0, x, v) = n_0(x)\, M(v).$$

The constant function on V is chosen as the equilibrium $M(v) = \frac{1}{|V|}$, and the kernels T_0, T_1, and T_2 satisfying this assumptions are written as

$$T_0(v, v') = \kappa M(v), \quad T_1(S, v, v') = v\nabla S, \ \textit{and}\ T_2(m, v, v') = v\nabla m,$$

then the operator $\mathcal{T}_0$ reads

$$\mathcal{T}_0(f) = \frac{\sigma}{|V|}\Big(\langle f\rangle - f(v)\Big).$$

For the stochastic case, we assume that $\sigma_i(u_i) = \lambda u_i$, we perform 100 realizations of the process, and we use ρ_m ($\rho = u_i$) to denote the realizations obtained for $m = 1, 2, \cdots, 100$. We are interested in the mean solution

$$\bar{\rho} = \mathbb{E}(\rho) = \frac{1}{100}\sum_{m=1}^{100}\rho_m,$$

where $u_1 = n$, $u_2 = m$, and $u_3 = S$.

In Figure 2, we present the plots in log scale of the error estimates given by

$$e_{\Delta x}(f) = \frac{\|f_{\Delta x}(t) - f_{2\Delta x}(t)\|_2}{\|f_{2\Delta x}(0)\|_2}$$

to test the convergence of the deterministic micro–macro scheme, and the mean l^2 norm defined by

$$\mathbb{E}[e_{\Delta x}(f)] = \mathbb{E}\Big[\frac{\|f_{\Delta x}(t) - f_{2\Delta x}(t)\|_2}{\|f_{2\Delta x}(0)\|_2}\Big]$$

is obtained after R realizations of the processes for the stochastic micro–macro scheme. This can be considered as an estimation of the relative error in the l^2 norm, where $f_{\Delta x}$ is the numerical solution computed with a grid of size $\Delta x = \frac{x_{max} - x_{min}}{N_x}$. The computations are performed with $N_x = \{100, 200, 400, 800, 1600\}$, $\Delta t = \frac{\Delta x^2}{2}$ at $t = 0.1$ for $\varepsilon = \{1, 10^{-2}, 10^{-6}\}$. We observe that, in both the deterministic and stochastic cases, the scheme demonstrates uniform convergence, as its time step remains independent of ε. For the deterministic case (Figure 2 (left)), we see first-order convergence in the kinetic regime and second-order convergence in the diffusive regime, consistent with the expected order of accuracy, since $\Delta t = O(\Delta x^2)$. Conversely, for the stochastic case (Figure 2 (right)), the observed convergence order is approximately 0.5 in the diffusive regime and 0.1 in the kinetic regime, which is lower than anticipated.

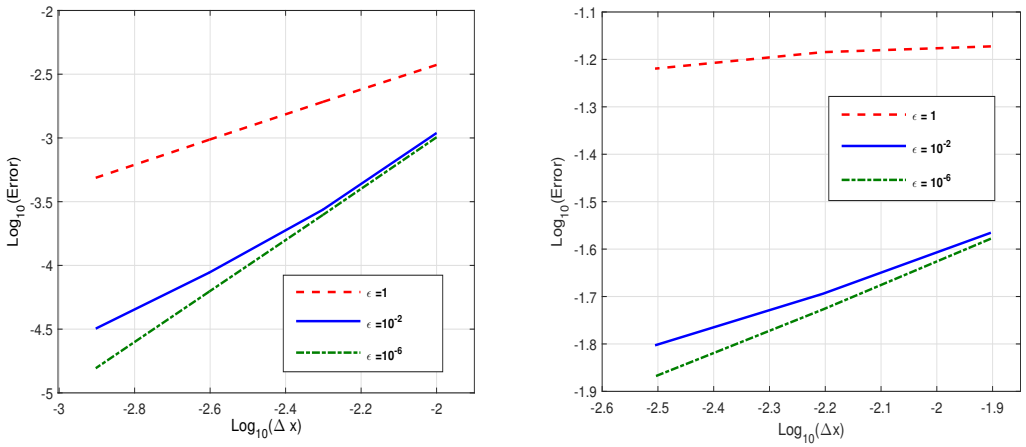

Figure 2. Convergence order of the deterministic scheme $\lambda = 0$ (left) vs. the stochastic scheme $\lambda = 0.1$ (right) for different values of ε at time $t = 0.1$ for cancer cell density.

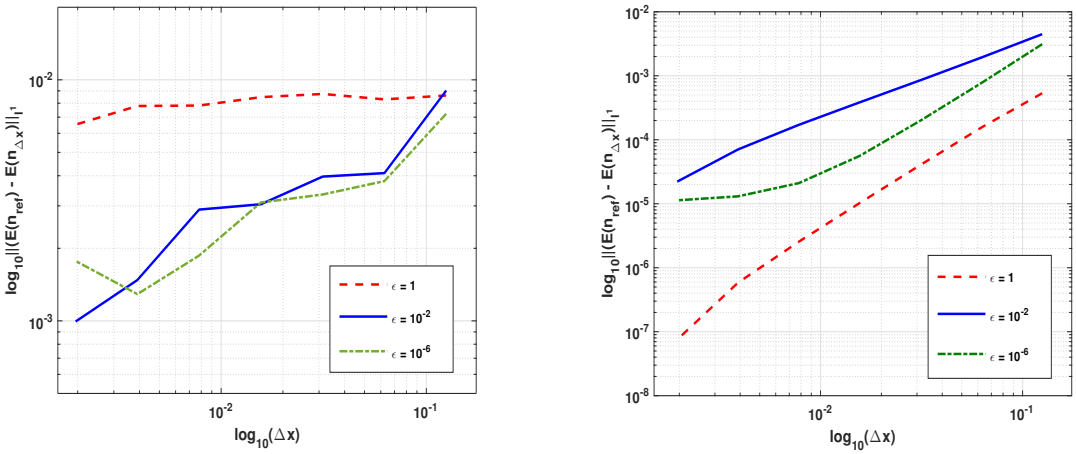

Figure 3. The convergence of the deterministic scheme with $\lambda = 0$ (left) vs. the stochastic scheme with $\lambda = 0.1$ (right) for different values of ε at time $t = 0.1$ for cancer cell density.

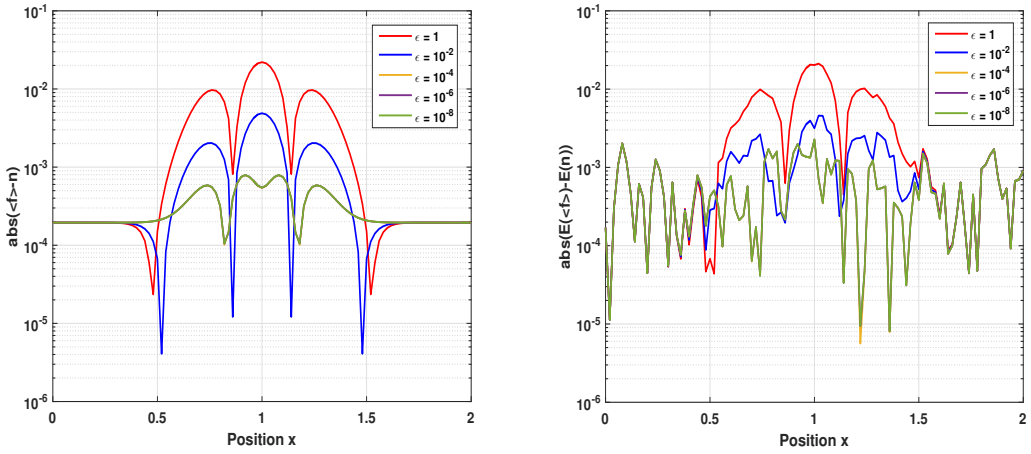

Figure 4. Convergence toward the macroscopic deterministic solution with $\lambda = 0$ (left) vs. the macroscopic stochastic solution $\lambda = 0.1$ (right) for different values of ε at time $t = 0.1$ for cancer cell density.

In order to check the numerical convergence of our method, since we do not have an analytic solution, we compute the mean reference solutions $\mathbb{E}(n_{h_{ref}})$ after 100 realizations of the process, using a fine mesh size $h_{ref} = 2^{-10}$. In Figure 3, we evaluate the convergence of the mean solutions $\mathbb{E}(n_h)$ from a coarse mesh size toward the mean reference solution. We also checked the convergence of the solutions of the kinetic theory model toward the solutions of the limiting macroscopic system. It can be seen in Figure 4 that, as $\varepsilon \to 0$, the densities computed via the micro–macro scheme approach those computed via the limiting macroscopic scheme.

We now set $N_x = 150$. The time step is set to $\Delta t = 1e - 04$. Figures 5 and 6 show the behavior at different regimes of the deterministic scheme ($\lambda = 0$) and the stochastic scheme $\lambda = 0.1$, respectively, with different values of ε ($\varepsilon_k = 2^{-k}$, where ($k \in \{0, 1, 2, 3, 6\}$). The obtained densities of cells are plotted at different times $t = 0.5, 0.7, 1, 1.5$. We note that the deterministic and stochastic schemes are both stable and converge as $\varepsilon \to 0$. Moreover, it is clear that the mean densities obtained from the stochastic scheme seem to converge to the densities obtained with the deterministic scheme as time increases.

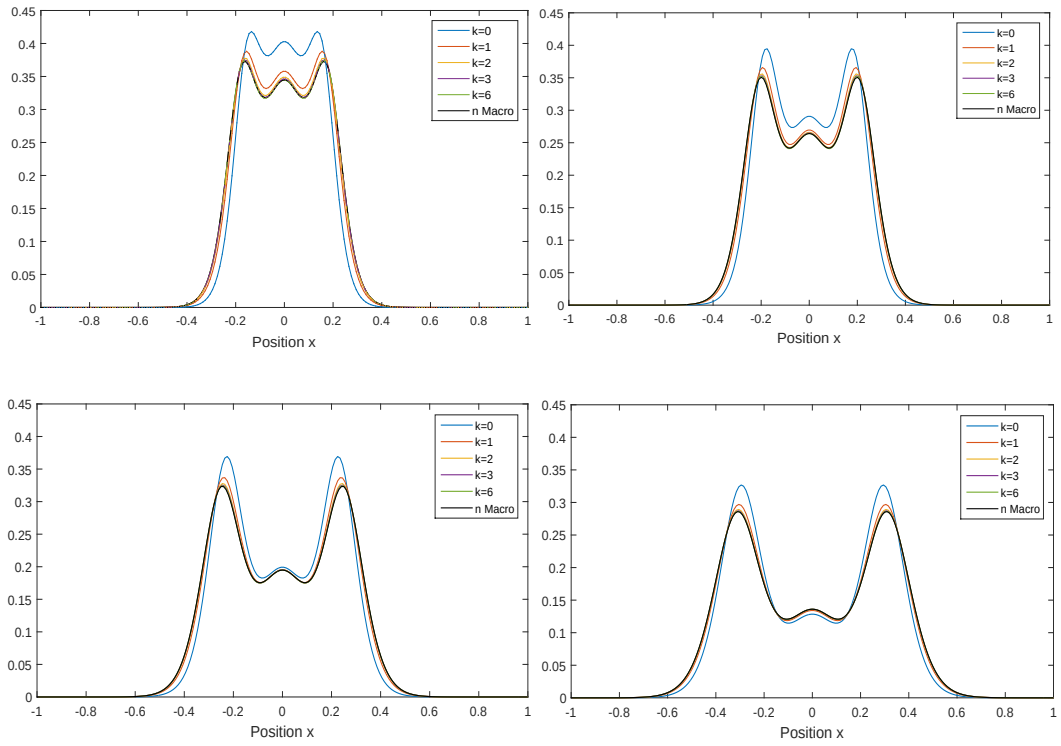

Figure 5. Deterministic case: Dynamics of the cancer cell densities obtained from the (AP) scheme with $\varepsilon = 2 \times 10^{-k}$, where $k = 0, 1, 2, 3, 6, 9$, versus the macroscopic scheme at successive times $t = 0.5, 0.7, 1, 1.5$. Parameter values: $\mu_1 = \mu_2 = 0$, and $\lambda = 0$.

In order to show the impact of the presence of proliferation and re-establishment terms in our model, we consider two cases. First, we neglect these terms by assuming that $\mu_1 = \mu_2 = 0$, and we provide, in Figure 7, the results of the behavior of cancer cell density, ECM density, and uPA concentration obtained from the asymptotic–preserving numerical scheme with $\varepsilon = 2 \times 10^{-6}$. It can be seen that chemotaxis and the uPA gradient direct cancer cells to regions with a high uPA concentration, while haptotaxis and the ECM gradient direct cancer's movement to high-density regions of the ECM. Second, we consider the presence of the proliferation and re-establishment terms by taking the parameters $\mu_1 = 0.05$ and $\mu_2 = 0.1$. In Figure 8, we observe that a large cluster of cancer cells has built up at the leading edge of the primary tumor at time $t = 1$. Moreover, the invading cluster of cancer cells has migrated all the way through the domain, driven mainly by the matrix-like protein vitronectin mediated by haptotaxis at time $t = 10$. Finally, at $t = 35$, most of the extracellular matrix has been degraded and cancer cells' locomotion is driven mainly by the uPA-mediated chemotaxis. Note that these results are consistent with those reported in [5].

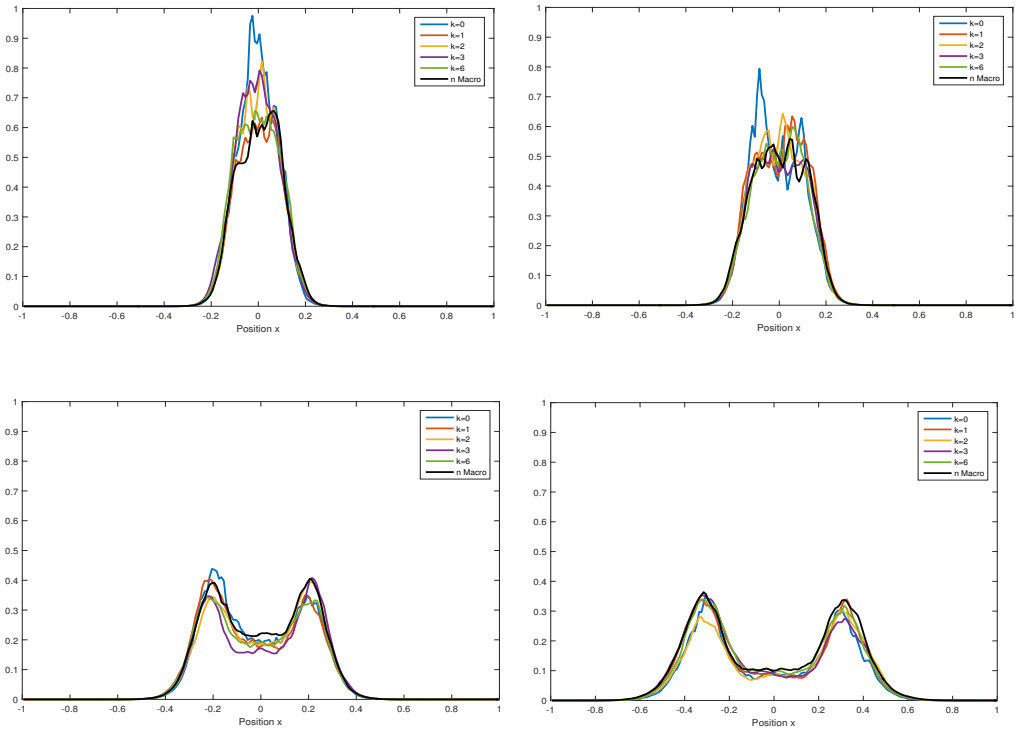

Figure 6. Stochastic case: Dynamics of the cancer cell densities obtained from the (AP) scheme with $\varepsilon = 2 \times 10^{-k}$, where $k = 0, 1, 2, 3, 6, 9$, versus the macroscopic scheme at successive times $t = 0.5, 0.7, 1, 1.5$. Parameter values: $\mu_1 = \mu_2 = 0$, and $\lambda = 0.1$.

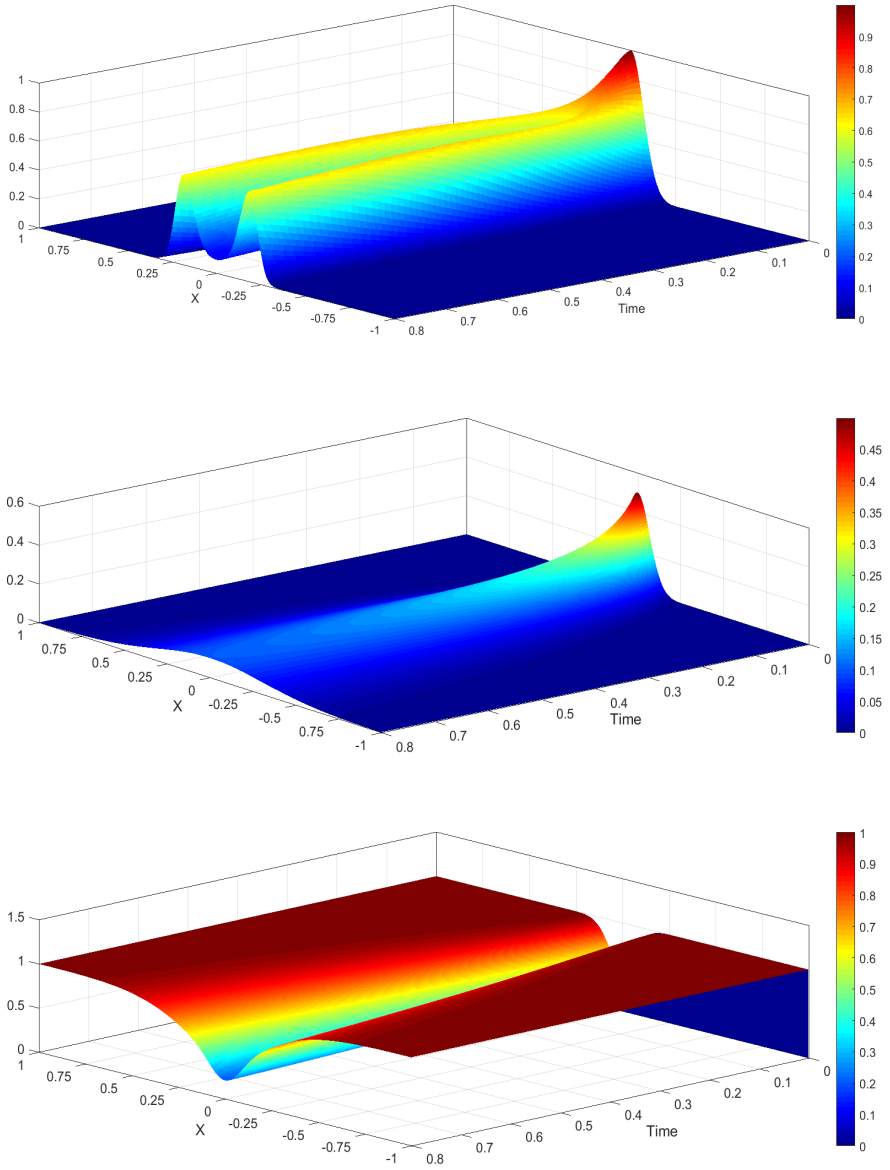

Figure 7. Evolution of the cancer cell density n, uPA concentration m, and ECM density S obtained from the asymptotic–preserving numerical scheme with $\varepsilon = 2 \times 10^{-6}$. Parameter values: $\mu_1 = \mu_2 = 0$, and $\lambda = 0$.

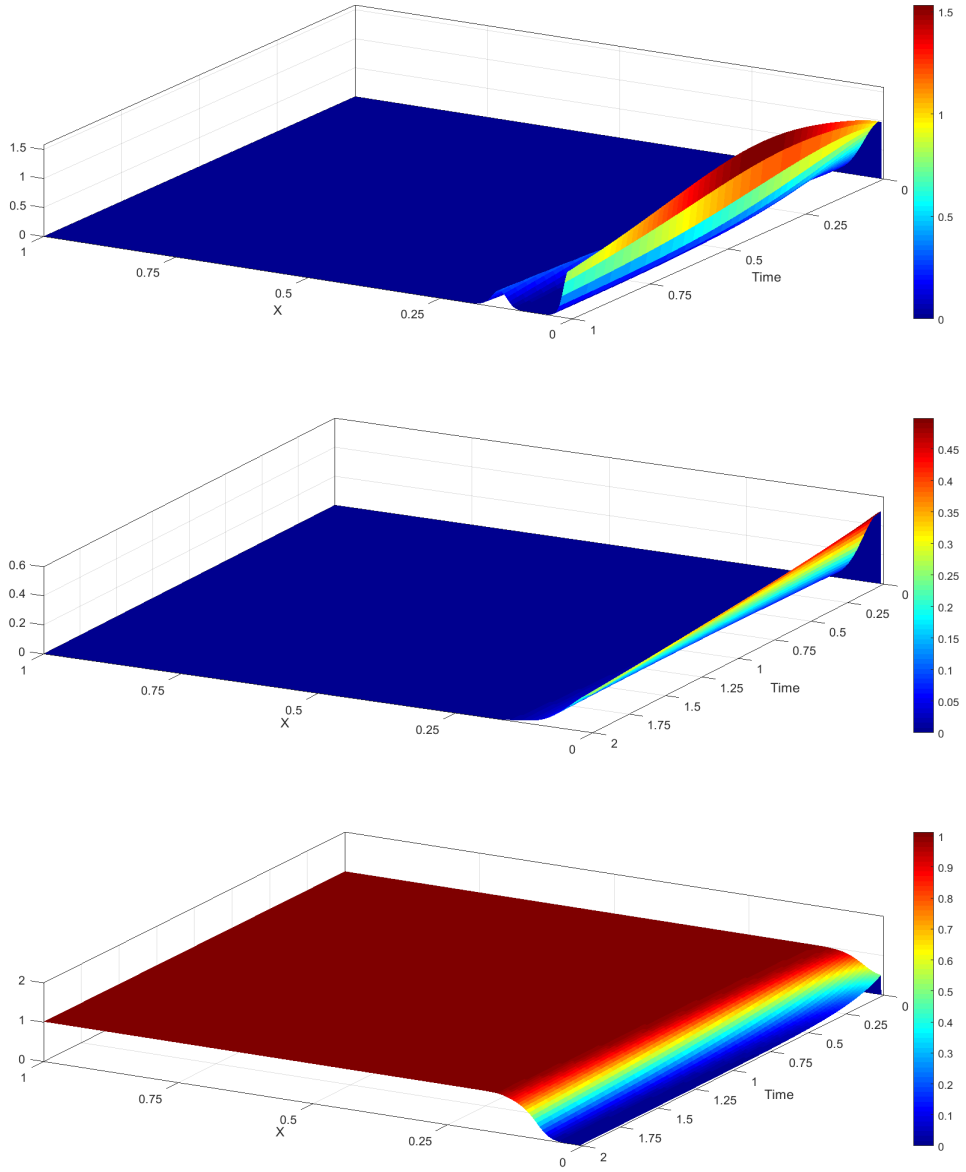

Figure 8. Evolution of the cancer cell density n, uPA concentration m, and ECM density S obtained from the asymptotic–preserving numerical scheme with $\varepsilon = 2 \times 10^{-6}$. Parameter values: $\mu_1 = 0.05$, $\mu_2 = 0.1$, and $\lambda = 0$.

4. Numerical simulation for the 2D macroscopic model

The following notations will be used for the description of the numerical scheme. Let D_R be a regular and admissible mesh of the domain D, constituting of open and convex polygons called control volumes with maximum size (diameter) h. For all $K \in D_R$, let x_K denote the center of K, $N(K)$ denote the set of the neighbors of K (i.e., the set of cells of D_R which have a common interface with K), and let $N_{\text{int}}(K)$ denote the set of the neighbors of K located in the interior of $\mathcal{D}_R$, $N_{\text{ext}}(K)$ denote the set of

edges of K on the boundary ∂D. Furthermore, for all $L \in N(K)$, $d(K, L)$ denotes the distance between x_K and x_L, $\sigma_{K,L}$ denotes the interface between K and L, by $\eta_{K,L}$ the unit normal vector to $\sigma_{K,L}$ outward to K. For all $K \in \mathcal{D}_R$, we use $|K|$ to denote the measure of K. The admissibility of D_R implies that $\overline{D} = \cup_{K\in D_R}\overline{K}$, $K \cap L = \emptyset$ if $K, L \in D_R$ and $K \neq L$, and a finite sequence of points $(x_K)_{K\in D_R}$ exists and the straight $\overline{x_K x_L}$ is orthogonal to the edge $\sigma_{K,L}$.

We now want to discretize the problems (1.2)–(1.8). Let Δt be the time step. We set $t^k = k\Delta t$. We start by taking the mean values on each K of the initial data in the following way:

$$n_K^0 = \frac{1}{|K|}\int_K n_0(x)dx, \quad m_K^0 = \frac{1}{|K|}\int_K m_0(x)dx \text{ and } S_K^0 = \frac{1}{|K|}\int_K S_0(x)dx. \tag{4.1}$$

Now it is natural to write a numerical approximation to our model (1.2) in the following way: for all $K \in D_R$ and $k \in [0, N-1]$

$$\begin{aligned}
n_K^{k+1} &= n_K^k - \frac{\Delta t}{|K|}\sum_{L\in N_K}\tau_{K,L}(D_n(n_K^k)Dn_{K,L}^{k+1}) + \frac{\Delta t}{|K|}\sum_{L\in N_K}\tau_{K,L}(\xi(m_K^k)n_K^{k+1}(Dm_{K,L}^k)^+ + \xi(m_L^k)n_L^{k+1}(Dm_{K,l}^k)^-)\\
&+\frac{\Delta t}{|K|}\sum_{L\in N_K}\tau_{K,L}(\chi(S_K^k)n_K^{k+1}(DS_{K,L}^k)^+ + \chi(S_L^k)n_L^{k+1}(DS_{K,l}^k)^-) + \mu_1\Delta t n_K^{n+1}(1 - n_K^n - S_K^n) + \sigma_1(n_K^k)\Delta W_1^k,\\
\gamma m_K^{k+1} &= \gamma m_K^k - \frac{D_m\Delta t}{|K|}\sum_{L\in N_K}\tau_{K,L}(Dm_{K,L}^{k+1}) + \Delta t(\alpha n_K^{k+1} - \beta m_K^k) + \gamma\sigma_2(m_K^k)\Delta W_2^k,\\
S_K^{k+1} &= S_K^k - \delta m_K^{k+1}S_K^{k+1} + \mu_2 S_K^{k+1}(1 - n_K^{n+1} - S_K^n) + \sigma_3(S_K^k)\Delta W_3^k,
\end{aligned} \tag{4.2}$$

where

$$\begin{gathered}
\tau_{K,L} = \tfrac{|\sigma_{K,L}|}{d(K,L)}, \quad Du_{K,L}^k = (u_L^k - u_K^k),\\
Du_{K,L}^k = 0 \text{ if } L \in N_{\text{ext}}(K),
\end{gathered} \tag{4.3}$$

$u^+ = \max(u, 0)$, $u^- = \max(-u, 0)$, and

$$\Delta W_i^k = W_i^{k+1} - W_i^k = \sqrt{\Delta t}\delta_k^i, \qquad i = 1, 2, 3$$

with δ_k^i being i.i.d. random variables with a normal distribution.

4.1. Numerical simulation

We perform the numerical simulation of the macroscopic chemotaxis–haptotaxis systems (1.2)–(1.8) in 2D space, using the finite volume method described above. The computation is performed in a square domain $[0, L] \times [0, L]$, discretized uniformly using rectangular volumes with a mesh size $h = 0.0125$. For the numerical simulations, we take the parameters set in Table 2 unless specified otherwise. The amplitude noise functions are taken as $\sigma_i(u_i) = \lambda u_i$, where λ is a positive constant. In our experiment, we consider a test related to the haptotaxis-only model. In this case, the dynamic of cancer cells is driven by the diffusion, haptotaxis, and noise. Therefore, we set $\xi_m = 0$. We provide

simulations results for the homogeneous ECM. To this end, the initial condition of tumor cells, the ECM and the uPA protease density are given by (see Figure 9)

$$n(x,y,0) = \exp(-400(x-0.5)^2-400(y-0.5)^2), \qquad m(x,y,0) = \frac{1}{2}n(x,y,0), \quad S(x,y,0) = 1-\frac{1}{2}n(x,y,0).$$

In the following, the simulation results are presented in the case of a homogeneous ECM. We also simulate the absence and presence of cell proliferation and/or the ECM's re-establishment. In Figure 10, we present numerical results showing the spatial evolution of the cancer cells' density and its interaction with the ECM by producing uPA, at several times ($t = 1,\ t = 5,\ t = 10,\ t = 15$), in the absence of uPA decay ($\beta = 0$), cell proliferation ($\mu_1 = 0$), and the ECM's re-establishment ($\mu_2 = 0$)). The effect of noise is observed in the heterogeneous spatial distribution of cells and the matrix degradation events (uPA), as well as the nonuniform degradation of ECM. Notably, the effect of haptotaxis with the degradation of the ECM is observed in the density of cancer cells, which decreases at the center of the domain where the ECM concentration is low, and the cells begin migrating towards regions with a higher ECM concentration over time. The presence of noise is further emphasized by the uneven spatial dispersion of the cell populations, leading to the fragmentation of the cancer cells. as it has been observed in experiments [48]. Compared with the uPA density, we observe that the tumor cells' density and ECM concentration exhibit higher oscillations, resulting in chaotic patterns.

In Figure 11, we show the simulation results in the presence of cancer cells proliferation, with $\mu_1 = 2$, whereas all other parameters are chosen as in the previous experiment. A fast invasion of cancer cells is observed, resulting in a fast degradation of the ECM, with the production of uPA. At time $t = 15$, almost all the domain is occupied by the cancer cells. The effect of noise is still highlighted by the heterogeneous spatial spreading of cancer cells and the chaotic patterns observed in ECM concentration.

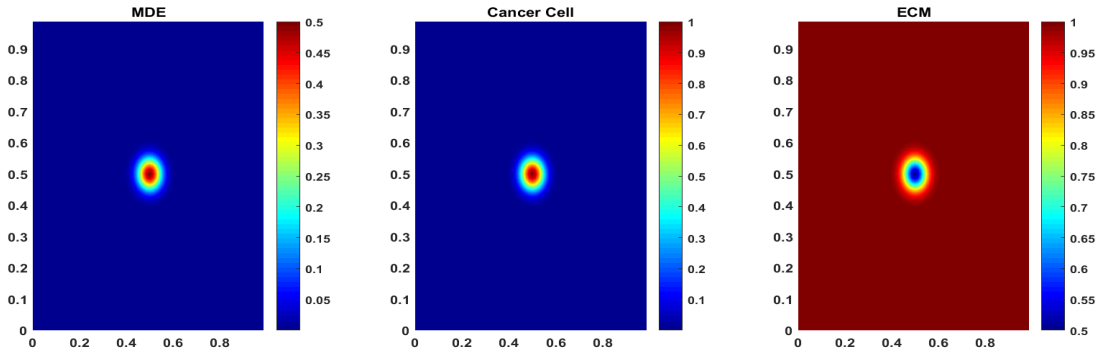

Figure 9. Initial conditions: Homogeneous extracellular matrix.

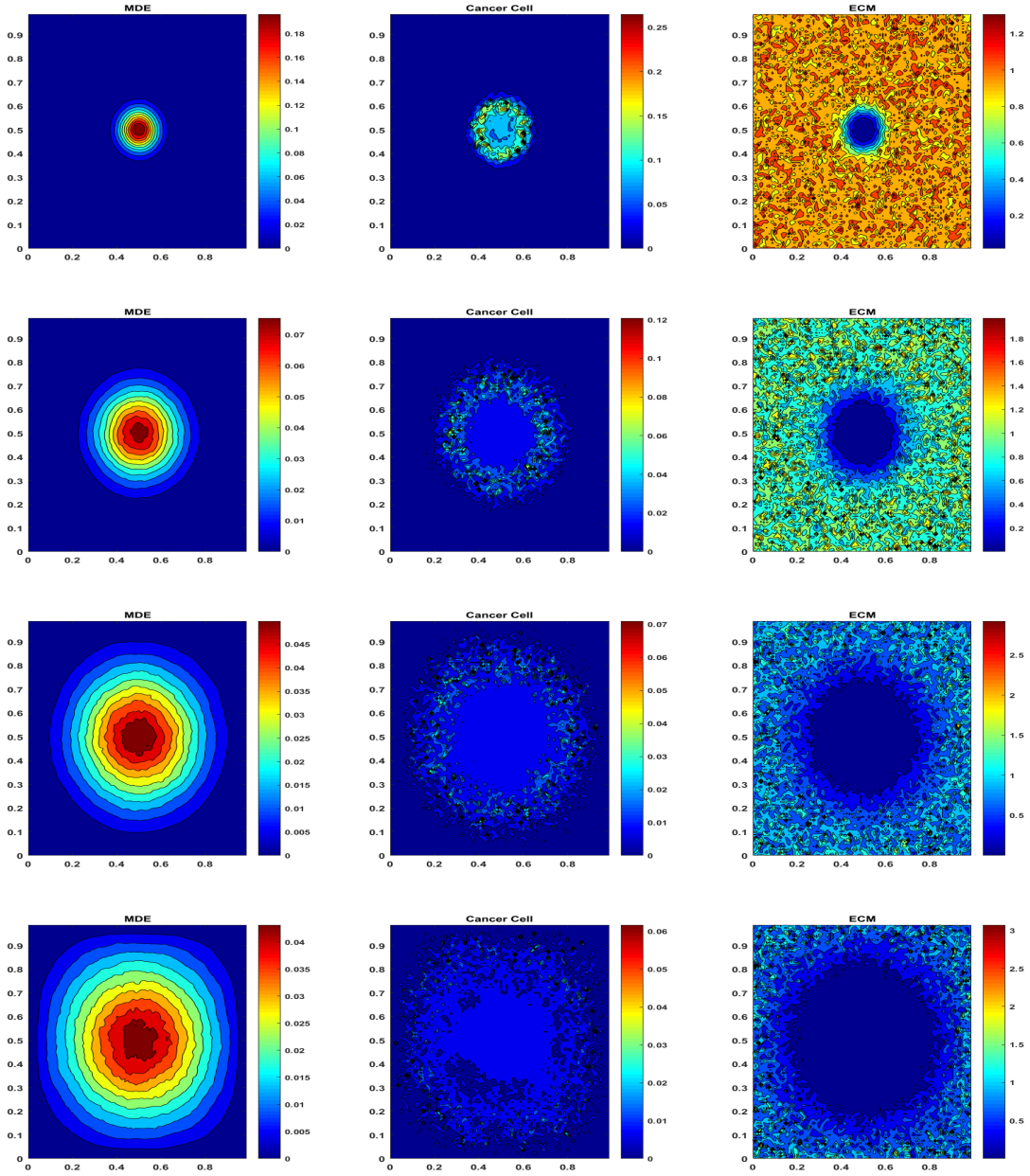

Figure 10. Spatio-temporal evolution in of the uPA concentration (left column), tumor cell density (middle column), and ECM density (right column), in absence of chemotaxis, cell proliferation, and the re-establishment of the ECM at successive times $t = 1, 5, 10, 15$. Parameter values: $\xi_m = \mu_1 = \mu_2 = 0$, and $\lambda = 0.1$.

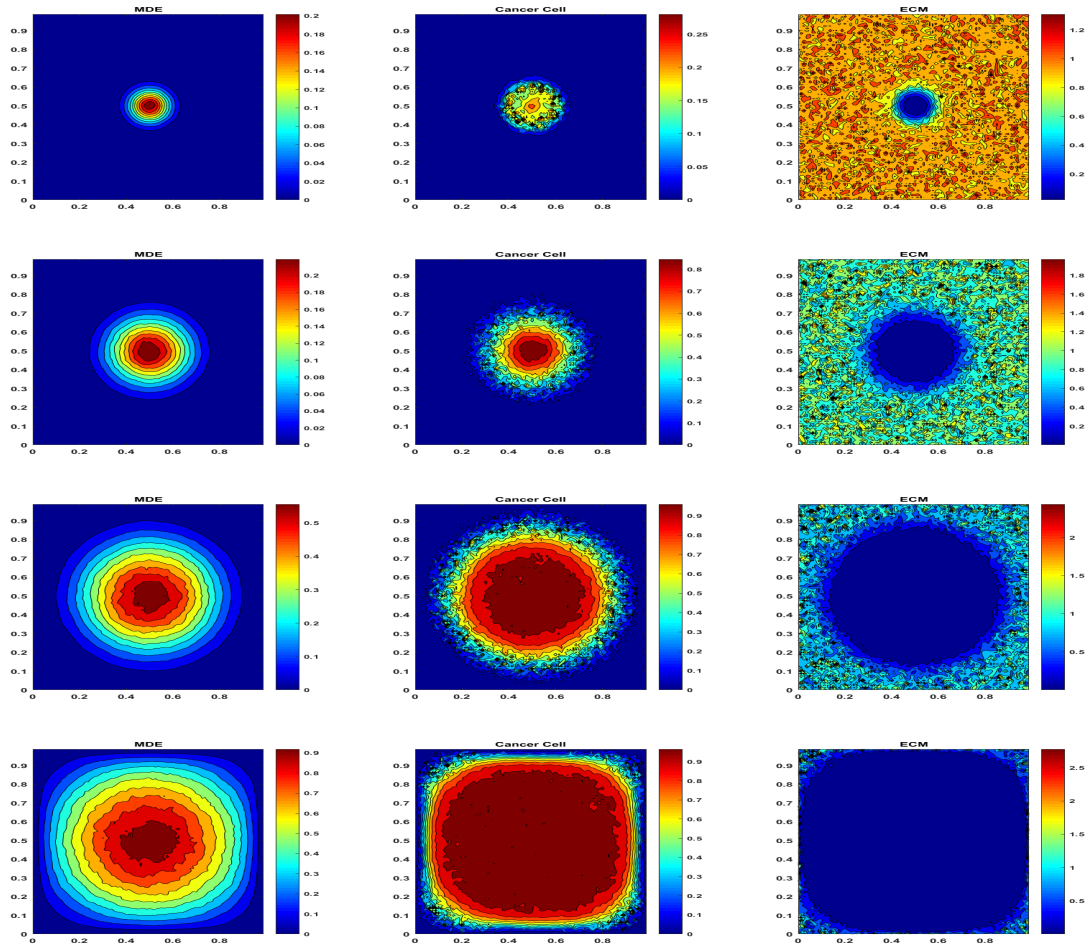

Figure 11. Spatio-temporal evolution of the uPA concentration (left column), tumor cell density (middle column), and ECM density (right column) with cell proliferation and without chemotaxis, and re-establishment of the ECM at successive times $t = 1,\ 5,\ 10,\ 15$. Parameter values: $\xi_m = \mu_2 = 0$, $\mu_1 = 2$, and $\lambda = 0.1$.

5. Conclusions and perspectives

This paper has been devoted to the multiscale derivation of a stochastic chemotaxis–haptotaxis system (1.2) by using the micro–macro decomposition method. The proposed numerical scheme is shown to be convergent and uniformly stable along the transition from kinetic to hydrodynamic regimes. Moreover, the macroscopic phenomena have been reproduced. Specifically, it is shown that in the case of the absence of the proliferation and re-establishment terms, chemotaxis and the uPA gradient direct cancer cells to regions of a high uPA concentration, while haptotaxis and the ECM gradient direct cancer's movement to high-density regions of the ECM. However, when those terms are considered, we observe throughout the evolution in time that a large cluster of cancer cells first builds up at the leading edge of the primary tumor. Next, the invading cluster of cancer cells migrates all the way through the domain, driven mainly by the matrix-like protein vitronectin, mediated by

haptotaxis. Then most of the ECM has been degraded, and cancer cells' locomotion is driven mainly by uPA-mediated chemotaxis. In addition, we have shown the effect of noise on the cell dynamics.

Looking ahead, we note that the micro–macro decomposition method developed in Section 2 leads to the derivation of the general model (2.12) of the angiogenesis phenomena. Note that we have derived the stochastic chemotaxis–haptotaxis system (1.2) with constant diffusion, with nonlinear diffusion (e.g., see [49]), and with nonlocal diffusion by typical choices of the operators T_i for $i = 0, 1, 2$ and the function ϕ. We are confident that it will be interesting to develop this micro–macro technique using the kinetic theory of active particles, which gives a better model of the cell-cell interactions and additional knowledge on the activity of each cell, for further applications, such as, the virus ingections (see recent papers [50, 51]) and new angiogenesis phenomena, such as chemotaxis–haptotaxis coupled with fluid equations (e.g., the augmented Brinkman or Navier–Stokes equations). This is not a simple wish but it is a work in progress. Finally, it is worth mentioning that several potential extensions of the current model can be considered. These include the incorporation of anisotropic diffusion and mechanical effects, the modeling of treatment dynamics and the emergence of therapeutic resistance, the application to both real and synthetic experimental datasets, and the integration of hybrid methodologies that couple discrete and continuum modeling frameworks.

Use of AI tools declaration

The authors declare they have not used Artificial Intelligence (AI) tools in the creation of this article

Author contributions

All authors have contributed equally to the work.

Conflict of interest

The authors declare that they have no known competing financial interests or personal relationships that could have appeared to influence the work reported in this paper.

References

1. A. Gerisch, M. A. J. Chaplain, Mathematical modeling of cancer cell invasion of tissue: Local and non-local models and the effect of adhesion, *J. Theor. Biol.*, **250** (2008), 684–704. https://doi.org/10.1016/j.jtbi.2007.10.026
2. H. M. Byrne, Dissecting cancer through mathematics: From the cell to the animal model, *Nat. Rev. Cancer*, **10** (2010), 221–230. https://doi.org/10.1038/nrc2808
3. S. Aznavoorian, M. L. Stracke, H. Krutzsch, E. Schiffmann, L. A. Liotta, Signal transduction for chemotaxis and haptotaxis by matrix molecules in tumor cells, *J. Cell Biol.*, **110** (1990), 1427–1438. https://doi.org/10.1083/jcb.110.4.1427

4. M. A. J. Chaplain, G. Lolas, Mathematical modeling of cancer cell invasion of tissue: The role of the urokinase plasminogen activation system, *Math. Models Methods Appl. Sci.*, **15** (2005), 1685–1734. https://doi.org/10.1142/S0218202505000947

5. M. A. J. Chaplain, G. Lolas, Mathematical modeling of cancer cell invasion of tissue: Dynamic heterogeneity, *Netw. Heterog. Media*, **1** (2006), 399–439. https://doi.org/10.3934/nhm.2006.1.399

6. A. Friedman, G. Lolas, Analysis of a mathematical model of tumor lymph-angiogenesis, *Math. Models Methods Appl. Sci.*, **15** (2005), 95–107. https://doi.org/10.1142/S0218202505003915

7. R. A. Gatenby, E. T. Gawlinski, A reaction-diffusion model of cancer invasion, *Cancer Res.*, **56** (1996), 5745–5753.

8. G. Meral, C. Stinner, C. Surulescu, A multiscale model for acid-mediated tumor invasion: Therapy approaches, *IMA J. Appl. Math.*, **80** (2015), 1300–1321. https://doi.org/10.1093/imamat/hxu055

9. C. Stinner, C. Surulescu, M. Winkler, Global weak solutions in a pde-ode system modeling multiscale cancer cell invasion, *SIAM J. Math. Anal.*, **46** (2014), 1969–2007. https://doi.org/10.1137/13094058X

10. J. A. Adam, N. Bellomo, *A Survey of Models for Tumor-Immune System Dynamics*, Birkhäuser, Boston, 1996. https://doi.org/10.1007/978-0-8176-8119-7

11. N. Bellomo, A. Bellouquid, E. D. Angelis, The modeling of the immune competition by generalized kinetic (boltzmann) models: Review and research perspectives, *Math. Comput. Model.*, **37** (2003), 1131–1142. https://doi.org/10.1016/S0895-7177(03)80007-9

12. N. V. Mantzaris, S. Webb, H. G. Othmer, Mathematical modeling of tumor-induced angiogenesis, *J. Math. Biol.*, **49** (2004), 111–187. https://doi.org/10.1007/s00285-003-0262-2

13. Z. Szymańska, Analysis of immunotherapy models in the context of cancer dynamics, *Appl. Math. Comput. Sci.*, **13** (2003), 407–418.

14. N. Bellomo, A. Bellouquid, Y. Tao, M. Winkler, Toward a mathematical theory of keller-segel models of pattern formation in biological tissues, *Math. Models Methods Appl. Sci.*, **25** (2015), 1663–1763. https://doi.org/10.1142/S021820251550044X

15. K. Choi, M. J. Kang, Y. S. Kwon, A. F. Vasseur, Contraction for large perturbations of traveling waves in a hyperbolic-parabolic system arising from a chemotaxis model, *Math. Models Methods Appl. Sci.*, **30** (2020), 387–437. https://doi.org/10.1142/S0218202520500104

16. C. Jin, Global classical solution and boundedness to a chemotaxis–haptotaxis model with re-establishment mechanisms, *Bull. London Math. Soc.*, **50** (2018), 598–618. https://doi.org/10.1112/blms.12160

17. P. Y. Pang, Y. Wang, Global boundedness of solutions to a chemotaxis–haptotaxis model with tissue remodeling, *Math. Models Methods Appl. Sci.*, **28** (2018), 2211–2235. https://doi.org/10.1142/S0218202518400134

18. Y. Tao, M. Winkler, A chemotaxis–haptotaxis system with haptoattractant remodeling: Boundedness enforced by mild saturation of signal production, *Commun. Pure Appl. Anal.*, **18** (2019), 2047–2067. https://doi.org/10.3934/cpaa.2019092

19. C. Engwer, C. Stinner, C. Surulescu, On a structured multiscale model for acid-mediated tumor invasion: The effects of adhesion and proliferation, *Math. Models Methods Appl. Sci.*, **27** (2017), 1355–1390. https://doi.org/10.1142/S0218202517400188

20. T. Xiang, J. Zheng, A new result for 2d boundedness of solutions to a chemotaxis–haptotaxis model with/without sub-logistic source, *Nonlinearity*, **32** (2019), 4890–4911. https://doi.org/10.1088/1361-6544/ab41d5

21. N. Kolbe, J. Katuchová, N. Sfakianakis, N. Hellmann, M. Lukáčová-Medviďová, Numerical study of cancer cell invasion dynamics using adaptive mesh refinement: The urokinase model, preprint, arXiv:1408.0642.

22. Y. Epshteyn, Discontinuous galerkin methods for the chemotaxis and haptotaxis models, *J. Comput. Appl. Math.*, **224** (2009), 168–181. https://doi.org/10.1016/j.cam.2008.04.030

23. S. Ganesan, S. Lingeshwaran, Galerkin finite element method for cancer invasion mathematical model, *Comput. Math. Appl.*, **73** (2017), 2603–2617. https://doi.org/10.1016/j.camwa.2017.04.006

24. J. Manimaran, L. Shangerganesh, Solvability and numerical simulations for tumor invasion model with nonlinear diffusion, *Comput. Math. Methods*, **2** (2020), e1068. https://doi.org/10.1002/cmm4.1068

25. D. Balding, D. McElwain, A mathematical model of tumor-induced capillary growth, *J. Theoret. Biol.*, **114** (1985), 53–73. https://doi.org/10.1016/S0022-5193(85)80255-1

26. H. Joshi, M. Yavuz, O. Taylan, A. Alkabaa, Dynamic analysis of fractal-fractional cancer model under chemotherapy drug with generalized mittag-leffler kernel, *Comput. Methods Programs Biomed.*, **260** (2024), 108565. https://doi.org/10.1016/j.cmpb.2024.108565

27. U. Dobramysl, M. Mobilia, M. Pleimling, U. C. Täuber, Stochastic population dynamics in spatially extended predator-prey systems, *J. Phys. A*, **51** (2018), 063001. https://doi.org/10.1088/1751-8121/aa95c7

28. M. Bandyopadhyay, J. Chattopadhyay, Ratio-dependent predator-prey model: Effect of environmental fluctuation and stability, *Nonlinearity*, **18** (2005), 913–936. https://doi.org/10.1088/0951-7715/18/2/022

29. M. Bendahmane, H. N. Nzeti, J. Tagoudjeu, M. Zagour, Stochastic reaction-diffusion system modeling predator-prey interactions with prey-taxis and noises, *Chaos*, **33** (2023), 073103. https://doi.org/10.1063/5.0140102

30. G. D. Prato, A. Ichikawa, Optimal control of linear systems with almost periodic inputs, *SIAM J. Control Optim.*, **25** (1987), 1007–1019. https://doi.org/10.1137/0325055

31. C. Prévôt, M. Röckner, *A Concise Course on Stochastic Partial Differential Equations*, Springer, 2007.

32. T. Bose, S. Trimper, Stochastic model for tumor growth with immunization, *Phys. Rev. E*, **79** (2009), 051903. https://doi.org/10.1103/PhysRevE.79.051903

33. A. Bellouquid, J. Tagoudjeu, An asymptotic–preserving scheme for kinetic models for chemotaxis phenomena, *Commun. Appl. Ind. Math.*, **9** (2018), 61–75. https://doi.org/10.2478/caim-2018-0010

34. M. Bendahmane, J. Tagoudjeu, M. Zagour, Odd-even based asymptotic–preserving scheme for a 2d stochastic kinetic-fluid model, *J. Comput. Phys.*, **471** (2022), 111649. https://doi.org/10.1016/j.jcp.2022.111649
35. F. Filbet, P. Laurençot, B. Perthame, Derivation of hyperbolic models for chemosensitive movement, *J. Math. Biol.*, **50** (2005), 189–207. https://doi.org/10.1007/s00285-004-0286-2
36. A. Atlas, M. Bendahmane, F. Karami, D. Meskine, M. Zagour, Kinetic-fluid derivation and mathematical analysis of nonlocal cross-diffusion-fluid system, *Appl. Math. Model.*, **82** (2020), 379–408. https://doi.org/10.1016/j.apm.2019.11.036
37. M. Bendahmane, F. Karami, M. Zagour, Kinetic-fluid derivation and mathematical analysis of the cross-diffusion-brinkman system, *Math. Meth. Appl. Sci.*, **41** (2018), 6288–6311. https://doi.org/10.1002/mma.5139
38. N. Bellomo, A. Bellouquid, On the derivation of angiogenesis tissue models: From the micro-scale to the macro-scale, *Math. Mech. Solids*, **20** (2014), 1–12. https://doi.org/10.1177/1081286514544855
39. M. Bendahmane, F. Karami, M. Zagour, Multiscale derivation of deterministic and stochastic cross-diffusion models in a fluid: A review, *Chaos*, **34** (2024), 122101. https://doi.org/10.1063/5.0238999
40. S. Jin, Efficient asymptotic–preserving (ap) schemes for some multiscale kinetic equations, *SIAM J. Sci. Comput.*, **21** (1999), 441–454. https://doi.org/10.1137/S1064827598334599
41. A. Klar, Asymptotic-induced domain decomposition methods for kinetic and drift diffusion semiconductor equations, *SIAM J. Sci. Comput.*, **19** (1998), 2032–2050. https://doi.org/10.1137/S1064827595286177
42. N. Crouseilles, M. Lemou, An asymptotic–preserving scheme based on a micro–macro decomposition for collisional vlasov equations: Diffusion and high-field scaling limits, *Kinet. Relat. Models*, **4** (2011), 441–477. https://doi.org/10.3934/krm.2011.4.441
43. G. Dimarco, L. Pareschi, Asymptotic–preserving implicit-explicit Runge-Kutta methods for nonlinear kinetic equations, *SIAM J. Numer. Anal.*, **51** (2013), 1064–1087. https://doi.org/10.1137/12087606X
44. J. Jang, F. Li, J. M. Qiu, T. Xiong, Analysis of asymptotic–preserving dg-imex schemes for linear kinetic transport equations in a diffusive scaling, *SIAM J. Numer. Anal.*, **52** (2014), 2048–2072. https://doi.org/10.1137/130938955
45. M. Bennoune, M. Lemou, L. Mieussens, An asymptotic–preserving scheme for the kac model of the boltzmann equation in the diffusion limit, *Continuum Mech. Thermodyn.*, **21** (2009), 401–421. https://doi.org/10.1007/s00161-009-0116-2
46. A. Dietrich, N. Kolbe, N. Sfakianakis, C. Surulescu, Multiscale modeling of glioma invasion: From receptor binding to flux-limited macroscopic pdes, *Multiscale Model. Simul.*, **20** (2022), 685–713. https://doi.org/10.1137/21M1412104
47. J. A. Carrillo, B. Yan, An asymptotic–preserving scheme for the diffusive limit of kinetic systems for chemotaxis, *Multiscale Model. Simul.*, **11** (2013), 336–361. https://doi.org/10.1137/110851687

48. V. Andasari, A. Gerisch, G. Lolas, A. P. South, M. A. J. Chaplain, Mathematical modeling of cancer cell invasion of tissue: Biological insight from mathematical analysis and computational simulation, *J. Math. Biol.*, **63** (2011), 141–171. https://doi.org/10.1007/s00285-010-0369-1

49. P. Zheng, C. Mu, X. Song, On the boundedness and decay of solutions for a chemotaxis–haptotaxis system with nonlinear diffusion, *Discrete Contin. Dyn. Syst. A*, **36** (2016), 1737–1757. https://doi.org/10.3934/dcds.2016.36.1737

50. N. Bellomo, K. J. Painter, Y. Tao, M. Winkler, Occurrence vs. absence of taxis-driven instabilities in may-nowak model for virus infection, *SIAM J. Appl. Math.*, **79** (2019), 1990–2010. https://doi.org/10.1137/19M1250261

51. M. Winkler, Boundedness in a chemotaxis-may-nowak model for virus dynamics with mildly saturated chemotactic sensitivity, *Acta Appl. Math.*, **163** (2019), 1–17. https://doi.org/10.1007/s10440-018-0211-0

AIMS Press